BLINDED: Probing Parity-Violation with the Four-Point Correlation Function of BOSS Galaxies

Oliver H. E. Philcox[1,2,*]

[1] *Department of Astrophysical Sciences, Princeton University, Princeton, NJ 08540, USA*
[2] *School of Natural Sciences, Institute for Advanced Study, 1 Einstein Drive, Princeton, NJ 08540, USA*

NB: This copy of the manuscript was written *before* the data were revealed. All figures and numerical results (shown in blue) are those from a *fake* data-set, and do not represent the BOSS data.

Parity-violating physics occuring in the early Universe can leave detectable traces in late-time observables. Whilst vector- and tensor-type parity-violation can be observed in the cosmic microwave background and galaxy ellipticities through B-modes, scalar-type signatures arise only in the four-point functions and beyond. Here, we perform a blind test for parity-violation in the four-point correlation function (4PCF) of the BOSS CMASS galaxy sample, considering modes in the range $[20, 160]h^{-1}$Mpc centered at redshift $z = 0.57$. The parity-odd 4PCF contains no contributions from standard ΛCDM physics, and can be efficiently measured using recently developed estimators. Data are primarily analyzed using a non-parametric rank test; this compares the measured 4PCFs from BOSS to those of realistic simulations, avoiding the assumption of a Gaussian likelihood. We obtain a detection probability of 7.8%, indicating no evidence for parity-violation. We additionally perform a χ^2-based analysis, making use of a linear compression scheme to greatly reduce the 4PCF dimensionality without bias; in this case, the detection probability is 14.7%. Using these measurements, constraints can be placed on physical models that generate parity-violation (and thus a parity-odd 4PCF signature). As an example, we consider an inflationary coupling between the inflaton and a $U(1)$ gauge field, and place bounds on the corresponding gauge field energy density. With the advent of data from DESI, Euclid, and Roman, as well as other large-scale structure probes, constraints on parity-violation will tighten considerably, strengthening the bounds on a variety of physical models.

I. INTRODUCTION

A detection of parity-violation in cosmological observables would be a smoking gun for physics beyond the standard model, and could provide crucial insights into the nature of dark matter, dark energy, and inflation. In the conventional paradigm, all cosmological correlators are symmetric under the parity operator $\mathbb{P}$, since gravity (along with all other standard model interactions, except the weak force [1]) is $\mathbb{P}$-invariant. Despite this, a number of theoretical arguments suggest that parity-violating interactions *should* occur in the early Universe, most notably to source baryogenesis. Creation of the current baryon asymmetry requires a process which violates charge and parity conservation [2]; a possible route is via leptogenesis, which, if sourced by gravity, must be parity-violating [e.g., 3–6].

Additional sources of parity-violation include inflationary interactions involving the Chern-Simons term [e.g., 7–9], primordial magnetic fields [e.g., 10–12], vector perturbations generated by cosmic strings or defects [e.g., 13–15], and reheating [e.g., 16, 17], all of which leave distinctive imprints on late-time observables. Some evidence for these models was recently provided by [18], which claimed at 2.4σ detection of parity-violation in the cosmic microwave background (hereafter CMB). Whilst there is a strong possibility that the effect is instead caused by interstellar dust emission [19], it has nevertheless provided a resurgence of interest in these theories.

To constrain such phenomena, we require observables that are parity-sensitive. Common choices are vector and tensor quantities, such as B modes of the CMB [e.g., 20], or those of galaxy ellipticities [e.g., 21]. These satisfy $\mathbb{P}[B] = -B$, and can be combined in two-point correlators (e.g., TB and EB for the CMB, or EB for weak lensing). Barring contamination by systematics, the observables should have no contribution from standard ΛCDM physics, but can be sourced by effects such as birefringence (whereupon the plane of the photon polarization is coherently rotated between the surface of last scattering and the observer, as in [18]), gravitational wave chirality [e.g., 7, 22], and the physics of inflation [23]. Information is not limited to the two-point function, however; higher-order correlators such as TTB can give additional constraining power on effects such as birefringence [24].

* ohep2@cantab.ac.uk

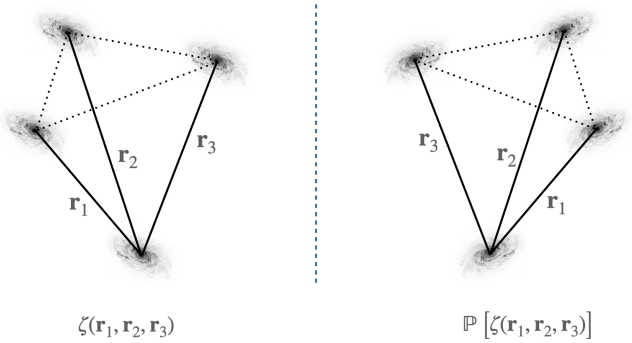

FIG. 1. Cartoon of the galaxy four-point correlation functions (4PCFs) considered in this work. In the left panel, we show the 4PCF, $\zeta(\boldsymbol{r}_1, \boldsymbol{r}_2, \boldsymbol{r}_3)$, which depends on the separation vectors of three secondary galaxies from a given primary. The right panel shows the parity-inverted 4PCF, $\mathbb{P}[\zeta(\boldsymbol{r}_1, \boldsymbol{r}_2, \boldsymbol{r}_3)]$, which corresponds to replacing $\boldsymbol{r}_i$ with $-\boldsymbol{r}_i$. Unlike for the 2PCF and 3PCF, the two configurations cannot be related by a rotation. The parity-even 4PCF is a sum of the two geometries (which have the same side-lengths and relative angles), whilst the parity-odd 4PCF is a difference. In the basis of §II A, these correspond to even and odd $\ell_1 + \ell_2 + \ell_3$ respectively. Assuming standard ΛCDM physics, the left and right correlators should be equivalent, thus the expectation value of the parity-odd 4PCF is zero.

When constructing observables from scalar fields (such as the galaxy density field or CMB temperature), obtaining a parity-sensitive quantity is more difficult. As an example, the isotropic galaxy two-point correlation function (hereafter 2PCF) is insensitive to parity, since the action of $\mathbb{P}$ is equivalent to a rotation, under which the statistic is invariant. In three-dimensions, the isotropic N-point correlation functions (NPCFs) are parity-sensitive only if $N > 3$; this applies also to the CMB, since the intrinsic fluctuations are the projection of a three-dimensional quantity. The simplest statistic with which to probe scalar parity-violation is thus the 4PCF, a cartoon of which is shown in Fig. 1. One caveat should be noted; large scale structure (LSS) correlators are sensitive also to redshift-space distortions [25, 26], giving dependence of the statistic on line-of-sight velocities [27]. This enables vector-type parity-violation to be probed in the 3PCF [28], though it requires careful modelling of galaxy velocities.

Whilst a number of works have considered the 4PCF of the CMB [e.g., 29, 30], including its parity-odd contributions [31], the LSS equivalent has been rarely explored. Given the influx of spectroscopic data expected in the next decade from DESI [32], Euclid [32], and Rubin [33], galaxy surveys seem to be a natural arena in which to hunt for parity-violating interactions, allowing constraints to exceed the CMB cosmic variance limit. Historically, use of the higher-point galaxy correlation functions has been hampered by the computational resources required for their estimation; naïvely, the 4PCF requires $\mathcal{O}(N_{\rm g}^4)$ operations to compute from $N_{\rm g}$ galaxies. Recent works have significantly improved upon this [34, 35], with the algorithm of [35] requiring only $\mathcal{O}(N_{\rm g}^2)$ operations. This allows the 4PCF of current galaxy surveys to be computed in $\sim$30 CPU-hours. The approach proceeds by first projecting the correlation function into a suitable angular basis [36]; thence, the integrals decouple and the 4PCF may be computed by summing over pairs of galaxies. This naturally generalizes to higher-dimensions, as well as to anisotropic correlators [37]. Furthermore, there is a natural split into parity-even and parity-odd basis functions. The former can be used to place constraints on gravitational non-Gaussianity from a hitherto unexplored statistic [38], whilst the latter are the subject of this work.

There are two main ways in which parity-violation can be probed using the galaxy 4PCF. Firstly, one may place constraints on the amplitudes of specific physical models given their associated theoretical predictions. This is an approach oft-used in the analysis of CMB 3- and 4-point functions, for example in non-Gaussianity studies, which typically exploit separability of the underlying theoretical templates for significant computational gain [e.g., 39]. A second method would be to first measure the *full* galaxy 4PCF (in some set of bins), then perform a blind test, looking for the signatures of *any* physical model (and systematic effects). This approach is possible since the parity-odd 4PCF receives no contribution in ΛCDM, including from general relativistic and baryonic effects. Given the multitude of possible models for parity-violation, we will principally adopt the second strategy in this work, though we demonstrate also the first, by placing constraints on a specific model involving Chern-Simons terms in the inflationary Lagrangian. Analysis using the galaxy 4PCF comes with its complexities, however. In particular, the high-dimensionality of the statistic prohibits conventional mock-based χ^2-analyses. To alleviate this, we include a data-compression step, facilitated using a theoretical model of the 4PCF covariance [40], which dramatically reduces the number of bins, without introducing bias. It is not guaranteed that the 4PCF distribution be Gaussian however [41, 42]; to provide a fully robust, yet conservative, test for parity-violation, we make use of a likelihood-free inference technique, involving

a suite of realistic simulations. The results below represent the first constraints on scalar parity-violation from LSS data.

The remainder of this work is structured as follows. In §II, we present the parity-odd 4PCF estimator, including the corrections necessary to account for non-uniform survey geometry, before we discuss the data and covariance matrices in §III. Analysis methods are considered in §IV, with the corresponding constraints on parity-violation presented in §V. §VI provides a motivating model for the parity-odd 4PCF, based on a Chern-Simons term in the inflationary Lagrangian, and whose amplitude is then bounded using the BOSS data. We conclude in §VII, with Appendix A sketching the derivation of the Chern-Simons 4PCF template. PYTHON code implementing our analysis pipeline on GitHub.[1]

Note on Blinding: To limit confirmation bias, the BOSS data were sent to an external collaborator (M. König) after computation, and not revealed until the analysis pipeline was constructed and tested. Furthermore, the manuscript was written with the BOSS data replaced by that from a single mock dataset, with only §V, §VI B & §VII modified post-unblinding.

II. MEASURING THE PARITY-ODD 4PCF

We begin by outlining our estimator for the parity-odd 4PCF, which is implemented in the public ENCORE code. Further details of the formalism can be found in [35] (for the general NPCF estimator and ENCORE), [36] (for the basis functions), [38] (for the parity-even 4PCF), and [37] (for extensions beyond flat 3D space).

A. Isotropic Basis Functions

Given a (scalar) density field $\delta(\boldsymbol{r})$, the 4PCF is defined as

$$\boxed{\zeta(\boldsymbol{r}_1,\boldsymbol{r}_2,\boldsymbol{r}_3) \equiv \langle \delta(\boldsymbol{s})\delta(\boldsymbol{s}+\boldsymbol{r}_1)\delta(\boldsymbol{s}+\boldsymbol{r}_2)\delta(\boldsymbol{s}+\boldsymbol{r}_3)\rangle\,,} \tag{1}$$

where $\langle\cdots\rangle$ represents a statistical average over realizations of δ. A cartoon of this parametrization is shown in Fig. 1. By statistical homogeneity, the 4PCF is independent of the absolute coordinate $\boldsymbol{s}$.

As demonstrated in [35, 37], a complete angular basis for the isotropic N-point correlation functions is given by the isotropic basis functions of $(N-1)$ coordinates defined in [36].[2] For $N=4$, the basis functions are

$$\mathcal{P}_{\ell_1\ell_2\ell_3}(\hat{\boldsymbol{r}}_1,\hat{\boldsymbol{r}}_2,\hat{\boldsymbol{r}}_3) \equiv (-1)^{\ell_1+\ell_2+\ell_3}\sum_{m_1m_2m_3}\begin{pmatrix}\ell_1 & \ell_2 & \ell_3\\ m_1 & m_2 & m_3\end{pmatrix} Y_{\ell_1m_1}(\hat{\boldsymbol{r}}_1)Y_{\ell_2m_2}(\hat{\boldsymbol{r}}_2)Y_{\ell_3m_3}(\hat{\boldsymbol{r}}_3), \tag{2}$$

where $Y_{\ell m}(\hat{\boldsymbol{r}})$ is a spherical harmonic, the 3×2 matrix is a Wigner 3-j symbol, and the m_i summations run over integer $m_i\in[-\ell_i,\ell_i]$. Such functions arise from the theory of angular momentum addition, and are specified by three non-negative integers $\{\ell_1,\ell_2,\ell_3\}$, encoding the relative orientation of $\hat{\boldsymbol{r}}_1,\hat{\boldsymbol{r}}_2$, and $\hat{\boldsymbol{r}}_3$. Due to the 3-j symbol, the integers must obey the triangle condition $|\ell_1-\ell_2|\leq\ell_3\leq\ell_1+\ell_2$, and we additionally enforce $\ell_i\leq\ell_{\rm max}$. In practice, we restrict to relatively low $\ell_{\rm max}$, which gives an angular resolution of $\theta_{\rm min}\approx 2\pi/\ell_{\rm max}$ for the internal angles of the 4PCF tetrahedron. The basis functions have the following properties under parity and conjugation transformations (for parity operator $\mathbb{P}$):

$$\mathbb{P}\left[\mathcal{P}_{\ell_1\ell_2\ell_3}(\hat{\boldsymbol{r}}_1,\hat{\boldsymbol{r}}_2,\hat{\boldsymbol{r}}_3)\right] = (-1)^{\ell_1+\ell_2+\ell_3}\mathcal{P}_{\ell_1\ell_2\ell_3}(\hat{\boldsymbol{r}}_1,\hat{\boldsymbol{r}}_2,\hat{\boldsymbol{r}}_3), \qquad \mathcal{P}^*_{\ell_1\ell_2\ell_3}(\hat{\boldsymbol{r}}_1,\hat{\boldsymbol{r}}_2,\hat{\boldsymbol{r}}_3) = (-1)^{\ell_1+\ell_2+\ell_3}\mathcal{P}_{\ell_1\ell_2\ell_3}(\hat{\boldsymbol{r}}_1,\hat{\boldsymbol{r}}_2,\hat{\boldsymbol{r}}_3), \tag{3}$$

implying that the basis is parity-odd and pure imaginary if $\ell_1+\ell_2+\ell_3$ is odd, and parity-even and real else. Furthermore, (2) is invariant under joint rotations of all three separation vectors, *i.e.* $\{\boldsymbol{r}_1,\boldsymbol{r}_2,\boldsymbol{r}_3\}\to\{R\boldsymbol{r}_1,R\boldsymbol{r}_2,R\boldsymbol{r}_3\}$, for arbitrary rotation matrix R.

The isotropic part of the galaxy 4PCF can be decomposed into the basis of (2):

$$\zeta_{\rm iso}(\boldsymbol{r}_1,\boldsymbol{r}_2,\boldsymbol{r}_3) = \sum_{\ell_1\ell_2\ell_3}\zeta_{\ell_1\ell_2\ell_3}(r_1,r_2,r_3)\mathcal{P}_{\ell_1\ell_2\ell_3}(\hat{\boldsymbol{r}}_1,\hat{\boldsymbol{r}}_2,\hat{\boldsymbol{r}}_3), \tag{4}$$

---

[1] Available at github.com/oliverphilcox/Parity-Odd-4PCF, upon paper acceptance.
[2] The approach naturally extends to *anisotropic* correlators [37], though we do not consider them in this work.

where the coefficients $\zeta_{\ell_1\ell_2\ell_3}$ (hereafter denoted 'multiplets') can be obtained via the orthonormality of $\mathcal{P}_{\ell_1\ell_2\ell_3}$.[3] Given the transformation properties of (3), we find a natural split of $\zeta_{\rm iso}$ into parity-even and parity-odd parts:

$$\zeta_+(\boldsymbol{r}_1,\boldsymbol{r}_2,\boldsymbol{r}_3) = \sum_{\ell_1+\ell_2+\ell_3=\text{even}} \zeta_{\ell_1\ell_2\ell_3}(r_1,r_2,r_3)\mathcal{P}_{\ell_1\ell_2\ell_3}(\hat{\boldsymbol{r}}_1,\hat{\boldsymbol{r}}_2,\hat{\boldsymbol{r}}_3), \tag{5}$$
$$\zeta_-(\boldsymbol{r}_1,\boldsymbol{r}_2,\boldsymbol{r}_3) = \sum_{\ell_1+\ell_2+\ell_3=\text{odd}} \zeta_{\ell_1\ell_2\ell_3}(r_1,r_2,r_3)\mathcal{P}_{\ell_1\ell_2\ell_3}(\hat{\boldsymbol{r}}_1,\hat{\boldsymbol{r}}_2,\hat{\boldsymbol{r}}_3).$$

These satisfy $\mathbb{P}\left[\zeta_\pm(\boldsymbol{r}_1,\boldsymbol{r}_2,\boldsymbol{r}_3)\right] = \pm\zeta_\pm(\boldsymbol{r}_1,\boldsymbol{r}_2,\boldsymbol{r}_3)$, and may be related to the sum and difference of the two panels in Fig. 1. In this work, we restrict to odd $\ell_1+\ell_2+\ell_3$, and thus consider the (purely imaginary) parity-odd 4PCF.

B. 4PCF Estimator

Invoking the ergodic principle, we may estimate the full 4PCF as an integral over four density fields,

$$\hat{\zeta}(\boldsymbol{r}_1,\boldsymbol{r}_2,\boldsymbol{r}_3) \equiv \frac{1}{V}\int d\boldsymbol{s}\,\delta(\boldsymbol{s})\delta(\boldsymbol{s}+\boldsymbol{r}_1)\delta(\boldsymbol{s}+\boldsymbol{r}_2)\delta(\boldsymbol{s}+\boldsymbol{r}_3), \tag{6}$$

where V is the integration volume. This is unbiased, *i.e.* it has expectation $\mathbb{E}[\hat{\zeta}] = \zeta$. Since the basis functions of (2) are orthonormal [36], (6) can be used to construct an estimator for the 4PCF basis coefficients:

$$\begin{aligned}\hat{\zeta}_{\ell_1\ell_2\ell_3}(r_1,r_2,r_3) &= \int d\hat{\boldsymbol{r}}_1 d\hat{\boldsymbol{r}}_2 d\hat{\boldsymbol{r}}_3\,\mathcal{P}^*_{\ell_1\ell_2\ell_3}(\hat{\boldsymbol{r}}_1,\hat{\boldsymbol{r}}_2,\hat{\boldsymbol{r}}_3)\hat{\zeta}(\boldsymbol{r}_1,\boldsymbol{r}_2,\boldsymbol{r}_3) \\ &= \frac{1}{V}\sum_{m_1m_2m_3}\begin{pmatrix}\ell_1 & \ell_2 & \ell_3\\ m_1 & m_2 & m_3\end{pmatrix} \\ &\quad\times\int d\boldsymbol{s}\,d\hat{\boldsymbol{r}}_1 d\hat{\boldsymbol{r}}_2 d\hat{\boldsymbol{r}}_3\,\delta(\boldsymbol{s})\delta(\boldsymbol{s}+\boldsymbol{r}_1)\delta(\boldsymbol{s}+\boldsymbol{r}_2)\delta(\boldsymbol{s}+\boldsymbol{r}_3)Y_{\ell_1m_1}(\hat{\boldsymbol{r}}_1)Y_{\ell_2m_2}(\hat{\boldsymbol{r}}_2)Y_{\ell_3m_3}(\hat{\boldsymbol{r}}_3),\end{aligned} \tag{7}$$

using the conjugate properties of (3). Defining the harmonic coefficients

$$\boxed{a_{\ell m}(\boldsymbol{s};r) \equiv \int d\hat{\boldsymbol{r}}\,\delta(\boldsymbol{s}+\boldsymbol{r})Y_{\ell m}(\hat{\boldsymbol{r}}),} \tag{8}$$

this is separable in $\hat{\boldsymbol{r}}_i$:

$$\boxed{\hat{\zeta}_{\ell_1\ell_2\ell_3}(r_1,r_2,r_3) = \sum_{m_1m_2m_3}\begin{pmatrix}\ell_1 & \ell_2 & \ell_3\\ m_1 & m_2 & m_3\end{pmatrix}\int\frac{d\boldsymbol{s}}{V}\delta(\boldsymbol{s})a_{\ell_1m_1}(\boldsymbol{s};r_1)a_{\ell_2m_2}(\boldsymbol{s};r_2)a_{\ell_3m_3}(\boldsymbol{s};r_3).} \tag{9}$$

For a discrete density field defined by $N_{\rm g}$ particles at positions $\{\boldsymbol{x}_i\}$ with weights w_i, the estimator can be written as a sum:

$$a_{\ell m}(\boldsymbol{x}_i;r) \equiv \sum_{j=1}^{N_{\rm g}} w_j Y_{\ell m}(\widehat{\boldsymbol{x}_j-\boldsymbol{x}_i})\delta_{\rm D}(r-|\boldsymbol{x}_j-\boldsymbol{x}_i|), \tag{10}$$
$$\hat{\zeta}_{\ell_1\ell_2\ell_3}(r_1,r_2,r_3) = \sum_{i=1}^{N_{\rm g}}\sum_{m_1m_2m_3}\begin{pmatrix}\ell_1 & \ell_2 & \ell_3\\ m_1 & m_2 & m_3\end{pmatrix} w_i a_{\ell_1m_1}(\boldsymbol{x}_i;r_1)a_{\ell_2m_2}(\boldsymbol{x}_i;r_2)a_{\ell_3m_3}(\boldsymbol{x}_i;r_3),$$

where the Dirac delta, $\delta_{\rm D}$, ensures that we count only secondary particles, j, separated from the primary, i, by a distance r. Since we must compute $a_{\ell m}$ at the location of each primary particle, the estimator requires a sum over pairs of particles, and thus has complexity $\mathcal{O}(N_{\rm g}^2)$; in practice, the scaling is closer to linear, as the m_i summation is rate limiting for large $\ell_{\rm max}$ [35]. By replacing the Dirac function in (10) by a binning function of finite width, the estimator extends to bin-averaged 4PCF estimates; we refer the reader to [35, 38] for details. We further note that the 4PCF contains also a 'disconnected' piece sourced by two copies of the 2PCF. Whilst this can be subtracted at the estimator level directly [38], it does not contribute to parity-odd multiplets, and will thus be ignored henceforth.

---

[3] Since the anisotropic basis functions are orthogonal to those of (2), the decomposition in (4) holds regardless of whether the full statistic is isotropic.

C. Edge-Correction

Finally, estimator (9) must be modified to account for the non-uniform survey geometry. For this purpose, we first define the 4PCF using the generalized Landy-Szalay form [35, 43, 44]

$$\hat{\zeta}(\boldsymbol{r}_1,\boldsymbol{r}_2,\boldsymbol{r}_3) \equiv \frac{\mathcal{N}(\boldsymbol{r}_1,\boldsymbol{r}_2,\boldsymbol{r}_3)}{\mathcal{R}(\boldsymbol{r}_1,\boldsymbol{r}_2,\boldsymbol{r}_3)}, \tag{11}$$

where $\mathcal{N}$ and $\mathcal{R}$ are the 4PCF estimates obtained from 'data-minus-random' and random catalogs respectively, both of which are modulated by the survey window function. Following some algebra, the *edge-corrected* 4PCF multiplets are given by

$$\zeta_{\ell_1\ell_2\ell_3}(r_1,r_2,r_3) = \sum_{\ell_1'\ell_2'\ell_3'} \left[M^{-1}\right]^{\ell_1'\ell_2'\ell_3'}_{\ell_1\ell_2\ell_3}(r_1,r_2,r_3) \frac{\mathcal{N}_{\ell_1'\ell_2'\ell_3'}(r_1,r_2,r_3)}{\mathcal{R}_{000}(r_1,r_2,r_3)}, \tag{12}$$

defining the coupling matrix

$$\begin{aligned} M^{\ell_1'\ell_2'\ell_3'}_{\ell_1\ell_2\ell_3}(r_1,r_2,r_3) = \frac{(-1)^{\ell_1'+\ell_2'+\ell_3'}}{(4\pi)^{3/2}} \sum_{L_1L_2L_3} \frac{\mathcal{R}_{L_1L_2L_3}(r_1,r_2,r_3)}{\mathcal{R}_{000}(r_1,r_2,r_3)} \left[\prod_{i=1}^{3}\sqrt{(2\ell_i+1)(2L_i+1)(2\ell_i'+1)}\right] \begin{Bmatrix} \ell_1 & L_1 & \ell_1' \\ \ell_2 & L_2 & \ell_2' \\ \ell_3 & L_3 & \ell_3' \end{Bmatrix} \\ \times \begin{pmatrix} \ell_1 & L_1 & \ell_1' \\ 0 & 0 & 0 \end{pmatrix} \begin{pmatrix} \ell_2 & L_2 & \ell_2' \\ 0 & 0 & 0 \end{pmatrix} \begin{pmatrix} \ell_3 & L_3 & \ell_3' \\ 0 & 0 & 0 \end{pmatrix}, \end{aligned} \tag{13}$$

with the curly brackets indicating a Wigner 9-j symbol. This allows us to 'undo' the effects of non-uniform survey geometry by measuring the 4PCF multiplets of the random field $\mathcal{R}$.[4] Note that there are two manners in which an parity-odd ζ can be sourced: parity-odd $\mathcal{N}$ and parity-even $\mathcal{R}$, or parity-odd $\mathcal{R}$ and parity-even $\mathcal{N}$.[5] For this reason, it is imperative to restrict to parity-odd multipets only *after* performing edge-correction.

III. DATA

A. Data and Simulations

Our dataset comprises galaxies from the twelfth data-release (DR12) [46] of the Baryon Oscillation Spectroscopic Survey (BOSS), part of SDSS-III [47, 48]. The survey contains two samples, CMASS and LOWZ, of which we use the former. This contains 587 071 (216 041) galaxies in the Northern (Southern) galactic cap (hereafter denoted NGC and SGC), across a redshift range $z \in [0.43, 0.7]$ and an effective redshift of $z_{\rm eff} = 0.57$.[6] We use a fiducial cosmology $\{\Omega_m = 0.31, \Omega_b h^2 = 0.022, h = 0.676, \sigma_8 = 0.8, n_s = 0.96, \sum m_\nu = 0.06\,{\rm eV}\}$ to convert angles and redshifts to Cartesian coordinates [cf. 38, 49], and assign galaxy weights according to

$$w_{\rm tot} = (w_{\rm rf} + w_{\rm fc} - 1) w_{\rm sys} w_{\rm fkp}. \tag{14}$$

Here $w_{\rm rf}$, $w_{\rm fc}$, and $w_{\rm sys}$ correspond to redshift-failure, fiber-collision, and systematic weights respectively, with $w_{\rm fkp} = [1 + n(z)P_0]^{-1}$ being the well-known FKP weight [50] for background number density $n(z)$ and $P_0 = 10^4 h^{-3}{\rm Mpc}^3$. To model the survey geometry, we use the BOSS random catalogs, containing 50× more randoms than galaxies.

We additionally make use of a suite of $N_{\rm mocks} = 1000$ MultiDark-Patchy (hereafter 'Patchy') simulations [51, 52]. These are computed using an approximate gravity solver and calibrated to an N-body simulation, with halo occupation parameters adjusted such that the mocks well reproduce the BOSS two- and three-point statistics. These share the CMASS survey geometry and are assigned weights via

$$w_{\rm tot} = w_{\rm veto} w_{\rm fc} w_{\rm fkp}, \tag{15}$$

including the veto weight $w_{\rm veto}$. The mocks are generated with the parameter set $\{\Omega_m = 0.3071, \Omega_b h^2 = 0.02205, h = 0.6777, \sigma_8 = 0.8288, n_s = 0.96, \sum m_\nu = 0\,{\rm eV}\}$ and coordinates are converted using the BOSS fiducial cosmology.

---

[4] Note that this does not remove any geometry effects that couple to the *anisotropic* 4PCF, nor those coupling to the 4PCF multiplets with $\ell_i > L$, assuming an initial $\ell_{\rm max}$ of L. The former effect is expected to be small (and usually ignored for the 3PCF [e.g., 45]), and the latter is ameliorated by discarding all multiplets containing $\ell_i = L$ after edge-correction, justified by noting that the coupling matrix, M, is close to tridiagonal.

[5] This occurs since the product of 3-j symbols in the coupling matrix is zero unless $\ell_1 + \ell_2 + \ell_3 + \ell_1' + \ell_2' + \ell_3' + L_1 + L_2 + L_3$ is even.

[6] Data are publicly available at data.sdss.org/sas/dr12/boss/lss/.

B. 4PCF Estimates

One of the main drawbacks with higher-order NPCFs is their dimensionality. To characterize the 4PCF, we must specify three multiplet indices (ℓ_1, ℓ_2, ℓ_3) and three radial bins (r_1, r_2, r_3), which can lead to a statistic with a large number of (highly correlated) elements [35]. For this reason, we adopt a relatively coarse radial binning scheme using $N_r = 10$ linearly spaced radial bins in $[20, 160]h^{-1}$Mpc, giving $\Delta r = 14h^{-1}$Mpc. Furthermore, we enforce $r_2 > r_1 + \Delta r$ and $r_3 > r_2 + \Delta r$, to ensure that the the separation between any two galaxies in the 4PCF tetrahedron is at least Δr (cf. Fig. 1). This removes modes from the non-linear region; these are difficult to model and can be strongly affected by baryonic physics. For the angular binning, we fix $\ell_{\rm max} = 5$, leading to a total of 56 radial bins and 111 multiplets (both parity-odd and parity-even), hence 6 216 elements in the full 4PCF statistic. In the analysis of §IV, we use only the 23 multiplets with odd $\ell_1 + \ell_2 + \ell_3$ and $\ell_i \leq 4$, giving a total of $N_\zeta = 1\,288$ elements; the rest are required for edge-correction (§II C).

Computation of the 4PCF multiplets, $\zeta_{\ell_1\ell_2\ell_3}(r_1, r_2, r_3)$, is performed using the ENCORE code [35].[7] We separately measure the contributions from a random catalog and a set of 32 'data-minus-random' catalogs, each with 1.5× the galaxy density; the latter are averaged to form the $\mathcal{N}$ quantities entering the edge-correction equation (11), whilst the former give $\mathcal{R}$.[8] Using (12), the quantities are then combined to form the edge-corrected 4PCF multipoles.

For samples with similar number densities to BOSS, the runtime of ENCORE scales as $N_{\rm g} N_r^3 (\ell_{\rm max} + 1)^5$ [35], with computation dominated by the m_i summations of (10) rather than estimation of the harmonic coefficients $a_{\ell m}$ (which scales as $N_{\rm g}^2(1+\ell_{\rm max})^2$, albeit with a more modest prefactor). In practice, we parallelize computation using OpenMP, with each NGC (SGC) each simulation requiring $\sim 32\,(6)$ CPU-hours to analyze on a modern 16-core Intel processor, including edge-correction. In total, analysis of the BOSS data and 1000 Patchy mocks required ~ 40k CPU-hours. This is comparable to the computational costs of the 2PCF analysis in Ref. [55] (adjusting for the different number of mocks), and is facilitated by the efficient nature of the ENCORE algorithm. We display a selection of the measured 4PCF multiplets in Fig. 2.

C. Covariance Matrices

The Patchy mocks described in §III A can be used to form a sample covariance of the 4PCF statistic in the standard manner:

$$\hat{\mathsf{C}}_{\ell_1\ell_2\ell_3;\ell_1'\ell_2'\ell_3'}(r_1, r_2, r_3; r_1', r_2', r_3') = \frac{1}{N_{\rm mocks}} \sum_{i=1}^{N_{\rm mocks}} \left(\zeta^{(i)}_{\ell_1\ell_2\ell_3}(r_1, r_2, r_3) - \bar{\zeta}_{\ell_1\ell_2\ell_3}(r_1, r_2, r_3)\right) \times \left(\zeta^{(i)}_{\ell_1'\ell_2'\ell_3'}(r_1', r_2', r_3') - \bar{\zeta}_{\ell_1'\ell_2'\ell_3'}(r_1', r_2', r_3')\right), \tag{16}$$

where $\zeta^{(i)}$ represents the i-th 4PCF estimate (in the NGC or SGC region), and $\bar{\zeta}$ is the average over $N_{\rm mocks}$ realizations. Since the number of 4PCF bins exceeds the number of Patchy mocks, this is not invertible, making it difficult to perform traditional χ^2-based analyses. For this reason, we supplement the sample covariance with the analytic covariance described in [40]. Essentially, this computes:

$$\begin{aligned}\mathrm{Cov}(\boldsymbol{r}_1, \boldsymbol{r}_2, \boldsymbol{r}_3; \boldsymbol{r}_1', \boldsymbol{r}_2', \boldsymbol{r}_3') = &\int \frac{d\boldsymbol{s}}{V}\frac{d\boldsymbol{s}'}{V} \langle \delta(\boldsymbol{s})\delta(\boldsymbol{s}+\boldsymbol{r}_1)\delta(\boldsymbol{s}+\boldsymbol{r}_2)\delta(\boldsymbol{s}+\boldsymbol{r}_3)\delta(\boldsymbol{s}')\delta(\boldsymbol{s}'+\boldsymbol{r}_1')\delta(\boldsymbol{s}'+\boldsymbol{r}_2')\delta(\boldsymbol{s}'+\boldsymbol{r}_3')\rangle \\ &- \int \frac{d\boldsymbol{s}}{V} \langle \delta(\boldsymbol{s})\delta(\boldsymbol{s}+\boldsymbol{r}_1)\delta(\boldsymbol{s}+\boldsymbol{r}_2)\delta(\boldsymbol{s}+\boldsymbol{r}_3)\rangle \int \frac{d\boldsymbol{s}'}{V} \langle \delta(\boldsymbol{s}')\delta(\boldsymbol{s}'+\boldsymbol{r}_1')\delta(\boldsymbol{s}'+\boldsymbol{r}_2')\delta(\boldsymbol{s}'+\boldsymbol{r}_3')\rangle ,\end{aligned} \tag{17}$$

where the statistical expectations can be expanded using Wick's theorem to yield products of four 2PCFs. The covariance is then projected into the angular basis of §II A and simplified. The approach makes a number of assumptions:

- **Isotropy**: The 2PCF $\xi(\boldsymbol{r}) \equiv \langle \delta(\boldsymbol{s})\delta(\boldsymbol{s}+\boldsymbol{r})\rangle$ is assumed to be a function only of $|\boldsymbol{r}|$. This neglects redshift-space distortions, which have a non-trivial impact on the isotropic 4PCF covariance.
- **Gaussianity**: The expectations entering (17) strictly contain additional contributions from higher-order correlators such as the 3PCF.

---

[7] github.com/oliverphilcox/encore.

[8] If the algorithm's runtime scales as $N_{\rm g}^2$, this partitioning minimizes the Poisson error at fixed computational cost [53, 54]. In our case, the scaling is closer to linear, thus the total work is roughly independent of the partition size.

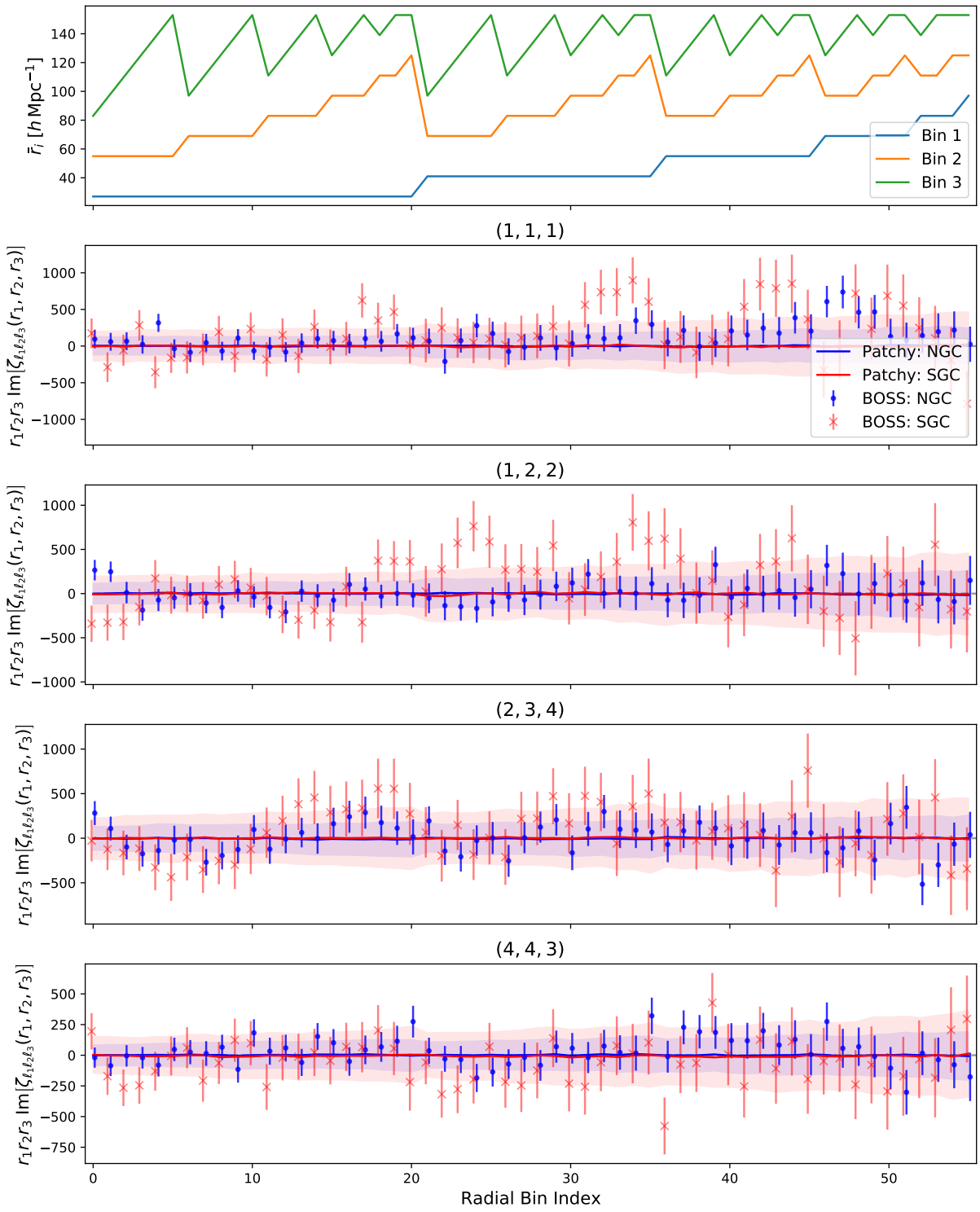

FIG. 2. Measurements of the parity-odd 4PCF from the BOSS CMASS galaxy sample, alongside those from 1000 Patchy simulations. The NGC (SGC) results are shown in blue (red) bands, with the BOSS data shown as error-bars, using the Patchy variances. Results are displayed for a selection of $\{\ell_1, \ell_2, \ell_3\}$ multiplets (which specify the internal angles of the galaxy tetrahedron, as in Fig. 1), whose values are indicated by the title of each subfigure. In total, 23 parity-odd multiplets are included in the analysis of §V. The horizontal axis specifies the radial bin combinations, $\{r_1, r_2, r_3\}$, with the linearly-averaged bin-centers plotted in the top panel. For visibility, the 4PCF measurements are rescaled by a factor $-i\, r_1 r_2 r_3$. As expected, the Patchy measurements show no signs of parity-violation. Furthermore, there is no obvious detection of parity-violation in the BOSS dataset; this is quantified in Figs. 4 & 5.

- **Survey Geometry**: Whilst the 4PCF is edge-corrected (§II C), the same is not true for the covariance. The latter inherits non-trivial dependence on the survey geometry [e.g., 56, 57], which cannot be simply captured by modifying the survey volume or shot-noise [40].

For these reasons, we do *not* expect the analytic models of [40] to accurately predict the true covariance of BOSS. It is a relatively close approximation however, and will thus be used as a proxy covariance to facilitate the analysis techniques described in §IV. We construct the covariance using the same radial binning parameters as in §III A, restricting to odd $\ell_1 + \ell_2 + \ell_3$. Following the prescription of [56] (but generalized to higher dimensions), we use an effective volume of $1.90h^{-3}\text{Gpc}^3$ ($0.77h^{-3}\text{Gpc}^3$) and shot-noise $P_{\text{shot}} = 3130h^{-3}\text{Mpc}^3$ ($3160h^{-3}\text{Mpc}^3$) for the NGC (SGC) subsample. The input 2PCFs are taken from a fit to the BOSS CMASS power spectrum, modelled using the Effective Field Theory of Large Scale Structure [58], as implemented in CLASS-PT [59].

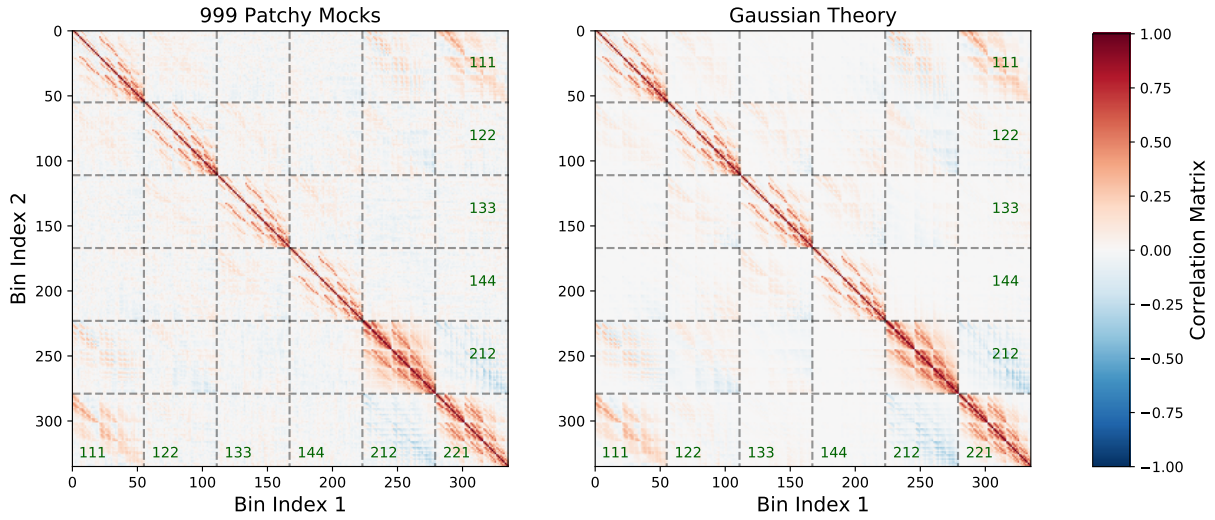

(a) Correlation Matrices

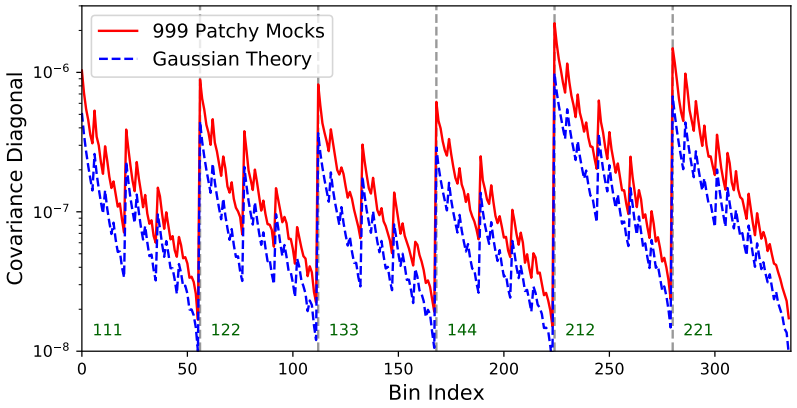

(b) Covariance Diagonal

FIG. 3. Comparison of the sample and analytic covariance matrices for the parity-odd 4PCF of the BOSS CMASS NGC region. The former are estimated using (16), whilst the latter use the approach of [40], which does not include redshift-space distortions, non-Gaussianity, or the effects of survey geometry. Fig. 3a compares the correlation matrices (defined as the covariance matrices normalized by their diagonals); we see similar structure in both cases. The rows and columns represent the indices of the 4PCF, collapsed into one dimension, with each submatrix (indicated by the dotted lines) showing a different multiplet $\{\ell_1, \ell_2, \ell_3\}$, as labelled in green. Elements within a submatrix are ordered in increasing radii r_1, r_2, r_3. We include only the first six multiplets here; 23 are used in the analysis of §V & VI B. Fig. 3b shows the corresponding diagonal elements of the covariance. Notably, the analytic covariance is an underestimate by a factor close to two; we expect this to arise primarily due to the non-uniform survey geometry of the CMASS region [40].

Fig. 3 compares the analytic and sample covariances for the NGC region, with the latter estimated from (16) using 1000 Patchy mocks. Considering the correlation matrices (Fig. 3a, defined as $\mathsf{R}_{ij} \equiv \mathsf{C}_{ij}/\sqrt{\mathsf{C}_{ii}\mathsf{C}_{jj}}$ for covariance C_{ij}),

we find good agreement between the two, indicating that the Gaussian theory model well reproduces the matrix structure. However, the diagonal elements (Fig. 3b) of the analytic covariance are roughly a factor of two less than those of the sample covariance. This is likely to arise from the non-trivial survey geometry of the BOSS CMASS region [40] and prohibits direct use of the analytic covariance as a model for the 4PCF statistics.[9]

IV. ANALYSIS TECHNIQUES

Below, we discuss two techniques that will be used to search for a signature of parity-violation in §V: (1) a non-parametric rank-test, which does not require the likelihood to be Gaussian, and (2) data compression followed by a mock-based χ^2-analysis. Both approaches use the smooth (but inaccurate) covariance matrix model of §III C to overcome the difficulties associated with the high-dimensionality of the 4PCF. To avoid confirmation bias, the pipeline implementing these techniques[10] was constructed before the BOSS data were unblinded.

A. Non-Parametric Rank Test

Non-parametric tests provide a powerful way to analyze data when the underlying likelihood is not known. Here, we consider a *rank test*, examining the null hypothesis of zero parity-odd 4PCF. To implement this, we first define a test statistic, computed on both the data and a set of mocks. The simulations are required to obey the null hypothesis (*i.e.* be parity-invariant) and have realistic noise properties. The test statistic measured from data is then compared to the empirical distribution obtained from the mocks, allowing construction of a detection significance. For example, if the data statistic exceeds that of 95% of the mocks, we may reject the null hypothesis at 95% confidence. The principal advantage of this approach is that it does not require a theoretical PDF for the test statistic, *i.e.* we do not have to assume the 4PCF to be a draw from some multivariate Gaussian. A limitation is that one cannot claim a detection at high significance; rather the maximal confidence level is $(1 - 1/N_{\rm mocks})$.

Below, we will use the following test statistic, dubbed the *pseudo-*χ^2:

$$\tilde{\chi}^2 \equiv \left[\zeta^T \tilde{\mathsf{C}}^{-1} \zeta\right]_{\rm NGC} + \left[\zeta^T \tilde{\mathsf{C}}^{-1} \zeta\right]_{\rm SGC}, \tag{18}$$

where ζ is the set of measured parity-odd 4PCF multipoles (treated as a N_ζ-dimensional vector), and $\tilde{\mathsf{C}}$ is the theoretical covariance matrix (§III C). If $\tilde{\mathsf{C}}$ is equal to the sample covariance (in the limit of infinite mocks), (18) reduces to the usual χ^2 statistic, given a fiducial model of zero parity-odd 4PCF and assuming the NGC and SGC regions to be independent. Whilst the covariances are not quite equal in practice (Fig. 3), we expect (18) to produce a close-to-optimal weighting for the data, particularly if the likelihood is close to Gaussian. Furthermore, since the pseudo-χ^2 statistic does not subtract off a mean, the rank test will naturally account for any spurious parity-odd contributions that are present in both Patchy and BOSS. These might arise from imperfections in the edge-correction routine or lightcone projection effects. To perform the test, we simply compute $\tilde{\chi}^2$ for BOSS and each of the $N_{\rm mocks} = 1000$ Patchy simulations (§III A), before assigning a detection significance from the Patchy PDF, as above.

B. Compressed Gaussian Analysis

A common trick when dealing with high-dimensional statistics is to apply some form of data compression [e.g., 60–63]. In general, this proceeds by projecting the data onto some (small) set of basis vectors, thus greatly reducing the dimensionality. When performing parameter inference, basis vectors are usually chosen to preserve the Fisher information matrix [e.g., 60, 62] or the log-likelihood [63]. Since our primary goal in this work is to search for signatures of parity-violation in a model-agnostic fashion, we adopt a somewhat different compression scheme, following [38, 61].

Here, we project the 4PCF onto a basis given by the eigenvectors of the theoretical covariance matrix (§III C). Explicitly, we define the projected statistic

$$v \equiv \mathsf{U}^T \zeta, \tag{19}$$

---

[9] Note that this discrepancy is *not* fully resolved by rescaling the theory covariance by a constant factor.
[10] Available at github.com/oliverphilcox/Parity-Odd-4PCF, upon paper acceptance.

where the orthogonal matrix U is specified by $\tilde{\mathsf{C}} = \mathsf{U}\Lambda\mathsf{U}^T$ for diagonal eigenvalue matrix Λ. The compressed statistic has covariance $\mathbb{E}\left[vv^T\right] = \mathsf{U}^T\mathsf{C}\mathsf{U}$, where C is the covariance of ζ; if the theory and analytic covariances agree, this is diagonal and equal to Λ. In practice, we expect the compressed coefficients to be almost independent.

To perform dimensionality reduction, we must restrict to a subset of the aforementioned basis vectors. Given that we have no prior on the shape of a parity-violating 4PCF signal, we cannot select the basis vectors based on signal-to-noise considerations (as in [38, 61]). Instead, we use the $N_{\rm eig}$ eigenvectors with smallest Λ_i, corresponding to the directions that can be most well measured. This highlights the benefits of using the *theoretical* covariance matrix to perform the projection; since the sample covariance does not have full rank, its smallest eigenvalues are not well defined.

Following selection of the basis vectors, we project both the BOSS data and the Patchy mocks into the $N_{\rm eig}$-dimensional subspace using (19). As in (16), we can form a sample covariance for v from the Patchy measurements:

$$\hat{\mathsf{C}}_{v,\alpha\beta} = \frac{1}{N_{\rm mocks}}\sum_{i=1}^{N_{\rm mocks}}\left(v_\alpha^{(i)} - \bar{v}_\alpha\right)\left(v_\beta^{(i)} - \bar{v}_\beta\right), \tag{20}$$

where $v_\alpha^{(i)}$ indicates the compressed 4PCF of the i-th mock, with $\alpha, \beta \in \{1, \ldots, N_{\rm eig}\}$. Assuming $N_{\rm mocks} > N_{\rm eig}$, the sample covariance has full rank (unlike the uncompressed 4PCF covariance), and is thus invertible. In the low-dimensional subspace, analysis centers around the following statistic:

$$\hat{T}^2 = v^T\hat{\mathsf{C}}_v^{-1}v, \tag{21}$$

where we have assumed zero mean, as in the null hypothesis. If v is assumed to be Gaussian distributed, $\hat{T}^2$ follows a χ^2-distribution with $N_{\rm eig}$ degrees of freedom in the limit of large $N_{\rm mocks}$. In practice, we must account for noise in the sample covariance $\hat{\mathsf{C}}_v$. A approach is to add the correction factor of [64, 65], leading to the modified statistic

$$\hat{H}^2 = f_H \times v^T\hat{\mathsf{C}}_v^{-1}v, \qquad f_H = \frac{N_{\rm mocks} - N_{\rm eig} - 2}{N_{\rm mocks} - 1}, \tag{22}$$

whose expectation is χ^2. $\hat{H}^2$ is then analyzed using a χ^2-distribution, assuming Gaussianity. However, this does not correctly treat the sample covariance noise, and results in a PDF which is too sharply peaked if $N_{\rm eig}$ is close to $N_{\rm mocks}$ [66]. Instead, one should analyze the $\hat{T}^2$ statistic (21) directly, using the PDF:

$$f_T(T^2; n, p) = \frac{\Gamma\left[(n+1)/2\right]}{\Gamma(p/2)\Gamma\left[(n-p+1)/2\right]}\frac{n^{-p/2}(T^2)^{p/2-1}}{(T^2/n+1)^{(n+1)/2}}, \tag{23}$$

where $n = N_{\rm mocks} - 1$, $p = N_{\rm eig}$, and Γ is the Gamma function [66]. When dealing with multiple independent datasets (*i.e.* the NGC and SGC 4PCF measurements), one may sum the two T^2 estimates; the resulting PDF is the convolution of two copies of (23), and is easily evaluated with a Fast Fourier Transform. This statistic will be adopted for the main analysis of §V to ensure that we do not claim a false detection of parity-violation.

Finally, we comment on the validity of our compression scheme. By the Eckart-Young theorem [67], the scheme is optimal (in terms of inverse-variance) in the limit of $\tilde{\mathsf{C}} = \mathsf{C}$ and a Gaussian covariance. Since the data and mocks are compressed in the same manner, it is unbiased for any choice of projection matrix U or dimension $N_{\rm eig}$. If too few basis vectors are used or if the theory covariance is far from the truth, the penalty (in the limit of large $N_{\rm mocks}$) is simply a reduced detection significance.[11] When using finite $N_{\rm mocks}$, increasing $N_{\rm eig}$ will also lead to increased noise in the covariance matrix $\hat{\mathsf{C}}_v$, somewhat lessening the detection significance. To incorporate these effects, a range of $N_{\rm eig}$ values will be considered in §V.

V. RESULTS

Given the above discussions, we may now proceed to assess whether the BOSS data contains signatures of parity-violation. Firstly, we consider the raw 4PCF measurements, displayed in Fig. 2 for a selection of multiplets $\{\ell_1, \ell_2, \ell_3\}$. As expected, the mean parity-odd 4PCF of Patchy is close to zero. This functions as a useful consistency test for

[11] This is easiest to show by considering the average χ^2 difference between some signal ζ_0 and the null hypothesis of $\mathbb{E}\left[\hat{\zeta}\right] = 0$. Without compression, $\Delta\chi^2 = \zeta_0^T\mathsf{C}^{-1}\zeta_0$, whilst following projection by some $N_\zeta \times N_{\rm eig}$ matrix U, $\Delta\chi^2_{\rm proj} = \zeta_0^T\mathsf{U}\left(\mathsf{U}^T\mathsf{C}\mathsf{U}\right)^{-1}\mathsf{U}^T\zeta_0$. If the projection is optimal, *i.e.* if U is the eigenvector matrix of C, then $\Delta\chi^2_{\rm proj,opt} = \sum_{i=1}^{N_{\rm eig}}\bar{\zeta}_{0,i}^2/\Lambda_i$ where $\bar{\zeta}_0 = \mathsf{U}^T\zeta_0$. Since $\bar{\zeta}_{0,i}^2 \geq 0$ and $\Lambda_i > 0$, it is clear that $\Delta\chi^2_{\rm proj,opt} \leq \Delta\chi^2$, with equality iff $N_{\rm eig} = N_\zeta$. A similar result holds in the more general case due to the properties of projection matrices; this is easily shown by rotating to a diagonal basis.

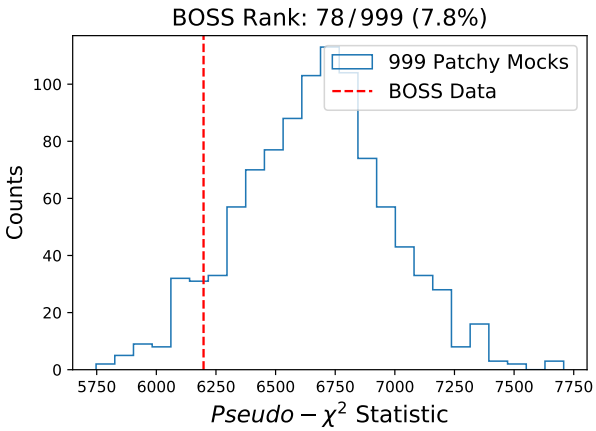

FIG. 4. Empirical distribution of the *pseudo*-χ^2 test statistic defined in (18) from 1000 Patchy mocks and the BOSS data. This is a proxy for the standard χ^2 parameter, but uses the theoretical covariance matrix of §III C. The data (shown as a vertical dashed line) has a CDF of 7.8%, which is fully consistent with the null hypothesis of zero parity-violation. Note that this test does not assume Gaussianity of the likelihood, and naturally encompasses any spurious parity-odd contributions appearing in both the Patchy mocks and the BOSS data. These could arise from imperfections in the window-function treatment.

the analysis pipeline; errors in the 4PCF computation could have led to a detectable signal, especially given that the parity-even 4PCF is large [38]. For the standard-deviations, we find a rough scaling of $(r_1 r_2 r_3)^{-1}$, with enhanced amplitudes found for the SGC region due to its smaller volume (§III). Moving to the BOSS results, we find considerable (correlated) scatter around zero, but no obvious signatures of parity-violation.

To examine this further, we turn to the non-parametric rank test of §IV A. In Fig. 4, we plot the empirical distribution of the *pseudo*-χ^2 test statistic; this appears to have broader tails than a standard χ^2 distribution (most likely due to imperfections in the theoretical covariance $\tilde{\mathsf{C}}$), highlighting the importance of a non-parametric treatment. The BOSS data has a rank of 78/1000, and an associated detection probability of 7.8%; this is fully consistent with a random draw from the empirical distribution. We report no evidence for parity-violation from this statistic.

An additional test is given by the projected χ^2-based analysis discussed in §IV B. Whilst this assumes a Gaussian distribution for the compressed statistic (somewhat justified by the reduced number of bins), it uses the sample covariance rather than the theoretical covariance, and thus optimally weights the data. In the top panel of Fig. 5, we show the theoretical and empirical distributions of the projected sample statistics T^2 and H^2 (§IV B) from Patchy, with the latter obtained via bootstrapping. Both statistics seem well-fit by their theory models, which is expected since $N_{\rm mocks}$ is considerably larger than $N_{\rm eig}$. In all cases, the BOSS statistic lies firmly within the central regions of the PDF, indicating a lack of evidence for parity-violation.

The detection probabilities are quantified in the lower panel of Fig. 5, using the CDFs of the χ^2 or T^2 distributions. For the T^2 statistic, the distribution of Patchy mocks appears uniform for all $N_{\rm eig}$ (as expected), whilst, for the H^2 statistic, we find some evidence of a discrepancy between the empirical and theoretical distributions. In particular, 83 mocks lie in the outermost 5% of the theory distribution, in contrast to the 50 ± 7 expected.[12] This echoes the conclusion of [66]; in the presence of covariance matrix noise, assuming a Gaussian likelihood for the summary statistic (and thus a χ^2 likelihood for H^2) may be dangerous, and could lead to false detections of parity-violation if $N_{\rm eig}$ is close to $N_{\rm mocks}$. Considering the BOSS results, we obtain detection significances of 46.7%, 34.1%, and 14.7% for $N_{\rm eig} = 10, 50$ and 100 respectively. Again, we do not find any evidence for parity-violation in this sample.

An interesting test is to remove the restriction on the radial bins introduced in §III B, instead including all bins satisfying $r_1 < r_2 < r_3$. In this case, secondary vertices of the 4PCF tetrahedra (Fig. 1) can be arbitrarily close together, which should lead to a slight increase in the information content. In this case, the non-parametric test gives a rank of 170/1000, with the $N_{\rm eig} = 100$ compressed χ^2-based analysis giving a detection probability of 34.0%. The inclusion of these short-scale modes does not source evidence for parity-violation.

To close, we comment on the variation of detection probabilities between the tests performed above. Differences between the non-parametric and compressed analyses are expected since we apply a different weighting to the data in each case (respectively, that of the inverse theoretical covariance and the inverse sample covariance). Furthermore, the fluctuations induced by changing $N_{\rm eig}$ can be justified by noting that different projections have different noise

[12] For the T^2 statistic, we find 62 such cases, which is more reasonable.

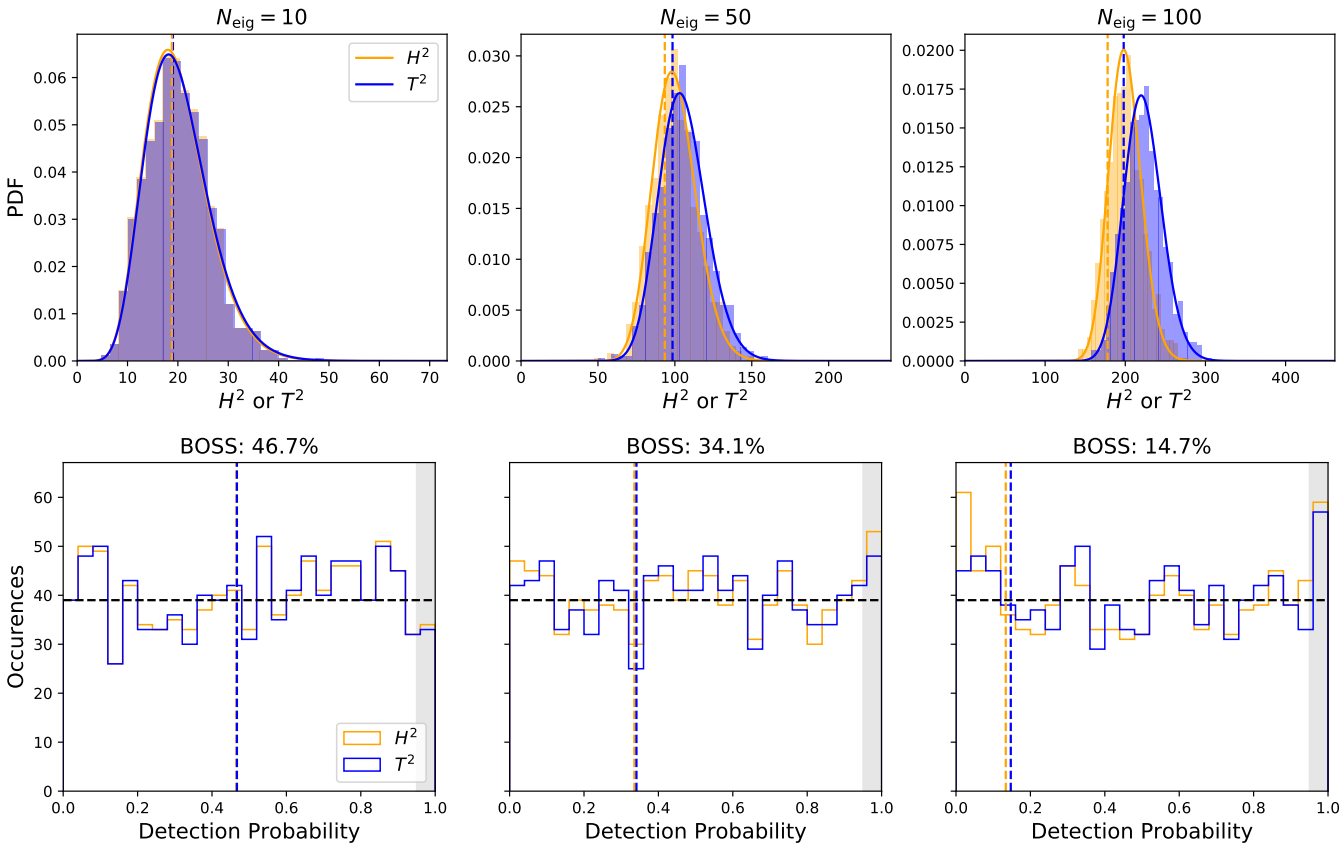

FIG. 5. Distributions of the H^2 and T^2 statistics (22) & (21) for the compressed BOSS data and Patchy simulations. We show results using various numbers of basis vectors, $N_{\rm eig}$, as indicated by the titles, and note that the statistic includes both NGC and SGC measurements. The top panels compare the theoretical and empirical PDFs for each statistic, whilst the bottom panels display the CDFs. Results for BOSS are shown as vertical dashed lines in both cases. To compute the empirical distributions (shown as histograms), we apply bootstrapping; $(N_{\rm mocks}-1)$ mocks are used to define a sample covariance, allowing computation of H^2 and T^2 for the excluded mock. The theoretical PDFs for H^2 and T^2 are the convolution of two χ^2 or T^2 distributions (23). For BOSS, we report detection probabilities of 46.7%, 34.1%, and 14.7% from the T^2 statistic using $N_{\rm eig} = 10$, 50, and 100 basis vectors respectively. We find no evidence for parity-violation (either physical or systematic-induced) in this sample.

properties, and thus should show different detection significances in the absence of a strong cosmological signal. Had the BOSS sample contained a clear signature of parity-violation, we would have expected it to appear in both tests; in that case, the detection significance in the compressed analysis should have decreased somewhat as $N_{\rm eig}$ was reduced (neglecting effects induced by covariance matrix noise). In this scenario, one would be tempted to construct a greater number of Patchy mocks in order to maximize the detection probability. We further note that the non-detection found herein provides an important consistency test for the BOSS analysis, since a non-zero parity-odd 4PCF could have been generated if the radial and angular selection functions were not well modelled (since these are not expected to obey parity conservation).

VI. AN INFLATIONARY MODEL FOR SCALAR PARITY-VIOLATION

The 4PCF measurements shown in §V may be used to place constraints on specific models of cosmological parity-violation. Below, we consider a single example, arising from a particular flavor of multi-field inflation, which gives an analytic form for the parity-odd galaxy 4PCF.

A. Modelling the Parity-Odd 4PCF

Consider an inflationary Lagrangian containing the following couplings between an inflaton field, ϕ, and a $U(1)$ gauge field, A_μ:

$$\mathcal{L} \supset f(\phi)\left[-\frac{1}{4}F_{\mu\nu}F^{\mu\nu} + \frac{\gamma}{4}F_{\mu\nu}\tilde{F}^{\mu\nu}\right], \tag{24}$$

where $F_{\mu\nu} \equiv \partial_\mu A_\nu - \partial_\nu A_\mu$ is a two-form. The second term involves the Hodge dual, $\tilde{F}^{\mu\nu}$, and is of the Chern-Simons form [e.g., 8]. Following [68], we assume constant γ and $f(\phi) \propto a^{-4}$ (for scale-factor a), such that the output spectra are close to scale-invariant. As shown in [31], the Chern-Simons term leads to a parity-violating trispectrum (as well as cosmic birefringence, [18]):

$$\left\langle \prod_{i=1}^{4}\zeta(\boldsymbol{k}_i)\right\rangle'_{\rm odd} = \left[t^{\boldsymbol{k}_1\boldsymbol{k}_2}_{\boldsymbol{k}_3\boldsymbol{k}_4} + \text{ 23 perms.}\right] \times (2\pi)^3\delta_{\rm D}\left(\sum_{i=1}^{4}\boldsymbol{k}_i\right), \tag{25}$$

where ζ is the primordial curvature perturbation, and the Dirac delta function enforces momentum conservation. Explicitly, this can be written

$$t^{\boldsymbol{k}_1\boldsymbol{k}_2}_{\boldsymbol{k}_3\boldsymbol{k}_4} = 3i\,A_{\rm CS}\,P_\zeta(k_1)P_\zeta(k_3)P_\zeta(s)\left[(\hat{\boldsymbol{k}}_1\times\hat{\boldsymbol{k}}_3)\cdot\hat{\boldsymbol{s}}\right]\left[1-\hat{\boldsymbol{k}}_1\cdot\hat{\boldsymbol{k}}_3+\hat{\boldsymbol{k}}_1\cdot\hat{\boldsymbol{s}}-\hat{\boldsymbol{k}}_3\cdot\hat{\boldsymbol{s}}\right] \equiv t(\boldsymbol{k}_1,\boldsymbol{k}_3,\boldsymbol{s}), \tag{26}$$

where $\boldsymbol{s}\equiv\boldsymbol{k}_1+\boldsymbol{k}_2$, and $P_\zeta(k)\approx H^2/(4\epsilon M_p^2k^3)$ is the power spectrum of curvature perturbations, for Hubble parameter H, Planck mass M_p, and slow-roll parameter ϵ. Assuming $|\gamma|>1$, the amplitude $A_{\rm CS}\geq 0$ can be related to standard inflationary parameters via

$$A_{\rm CS} \approx \frac{0.3}{\pi^2}\frac{e^{8\pi|\gamma|}}{|\gamma|^6}\frac{|g_*|}{0.01}\left(\frac{N}{60}\right)^2, \qquad g_* \approx -\frac{5.4\times10^5}{\pi}\frac{e^{4\pi|\gamma|}}{|\gamma|^3}\frac{0.01}{\epsilon}\left(\frac{N}{60}\right)^2\frac{\rho_E}{\rho_\phi}, \tag{27}$$

where ρ_E/ρ_ϕ is the ratio of the gauge field vacuum energy density to that of the inflaton, and we assume that modes of interest exited the horizon N e-folds before the end of inflation. Due to the presence of the cross-product in (26), the Chern-Simons trispectrum (and thus 4PCF) is parity-odd.[13] Notably a parity-even piece is also sourced (from the $f(\phi)F_{\mu\nu}F^{\mu\nu}$ term in 24), with the relative amplitude of the two controlled by the γ parameter. Since the parity-even trispectrum contains significant contributions from gravitational non-Gaussianity [38], we expect the parity-odd signature to be much easier to detect.

To place constraints on this interaction, we must compute the galaxy 4PCF associated with the primordial trispectrum of (26). At redshift z, the tree-level galaxy trispectrum, T_g, can be related to the primordial correlator via

$$(2\pi)^3\delta_{\rm D}(\boldsymbol{k}_1+\boldsymbol{k}_2+\boldsymbol{k}_3+\boldsymbol{k}_4)T_g(\boldsymbol{k}_1,\boldsymbol{k}_2,\boldsymbol{k}_3,\boldsymbol{k}_4,z) = \left\langle\prod_{i=1}^{4}Z_1(\boldsymbol{k}_i,z)M(k_i,z)\zeta(\boldsymbol{k}_i)\right\rangle, \tag{28}$$

where $M(k,z)$ is the transfer function, defined by $\delta_{\rm matter}(\boldsymbol{k},z)=M(k,z)\zeta(\boldsymbol{k})$, and $Z_1(\boldsymbol{k},z)\equiv b(z)+f(z)(\hat{\boldsymbol{k}}\cdot\hat{\boldsymbol{n}})^2$ is the tree-level galaxy RSD kernel (for linear bias $b(z)$, growth-rate $f(z)$ and line-of-sight $\hat{\boldsymbol{n}}$). From (28), we may obtain the 4PCF using Fourier transforms:

$$\begin{aligned}\zeta(\boldsymbol{r}_1,\boldsymbol{r}_2,\boldsymbol{r}_3,z) = \prod_{i=1}^{4}\left[\int_{\boldsymbol{k}_i}M(k_i,z)Z_1(\boldsymbol{k}_i,z)\right]\int_{\boldsymbol{s}}t(\boldsymbol{k}_1,\boldsymbol{k}_3,\boldsymbol{s})\left[e^{i(\boldsymbol{k}_1\cdot\boldsymbol{r}_1+\boldsymbol{k}_2\cdot\boldsymbol{r}_2+\boldsymbol{k}_3\cdot\boldsymbol{r}_3)}+\text{ 23 perms.}\right]\\ \times(2\pi)^3\delta_{\rm D}\left(\boldsymbol{k}_1+\boldsymbol{k}_2-\boldsymbol{s}\right)(2\pi)^3\delta_{\rm D}\left(\boldsymbol{k}_3+\boldsymbol{k}_4+\boldsymbol{s}\right),\end{aligned} \tag{29}$$

shifting the permutation sum to the exponential term by symmetry, and using Dirac delta functions to enforce $\boldsymbol{s}=\boldsymbol{k}_1+\boldsymbol{k}_2=-\boldsymbol{k}_3-\boldsymbol{k}_4$. The corresponding multiplets, $\zeta_{\ell_1\ell_2\ell_3}$, can then be estimated by performing weighted integrals over $\hat{\boldsymbol{r}}_i$, as in (7). Following a lengthy derivation sketched in Appendix A, we obtain the final form:

$$\begin{aligned}\zeta_{\ell_1\ell_2\ell_3}(r_1,r_2,r_3,z) = (4\pi)^{11}\sqrt{2}A_{\rm CS}\,i^{\ell_1+\ell_2+\ell_3}\sum_{L_1L_2L_3L_4L_5L_5'}i^{L_1+L_2+L_3+L_4-L_5+L_5'}\mathcal{C}_{L_1L_2L_3L_4L_5L_5'}\\ \times\begin{pmatrix}L_1&L_2&L_5\\0&0&0\end{pmatrix}\begin{pmatrix}L_3&L_4&L_5'\\0&0&0\end{pmatrix}\mathcal{M}^{\ell_1\ell_2(\ell_3)\ell_30}_{L_1L_2L_3L_4L_5L_5'}\\ \times\int x^2dx\int x'^2dx'\,K_{L_5L_5'}(x,x')I^{\ell_1}_{L_1}(x;r_1)J^{\ell_2}_{L_2}(x;r_2)I^{\ell_3}_{L_3}(x';r_3)J^0_{L_4}(x';0)+23\text{ perms.}\end{aligned} \tag{30}$$

[13] This is as expected, since the Lagrangian involves a pseudo-scalar field ϕ and a dual $\tilde{F}^{\mu\nu}$.

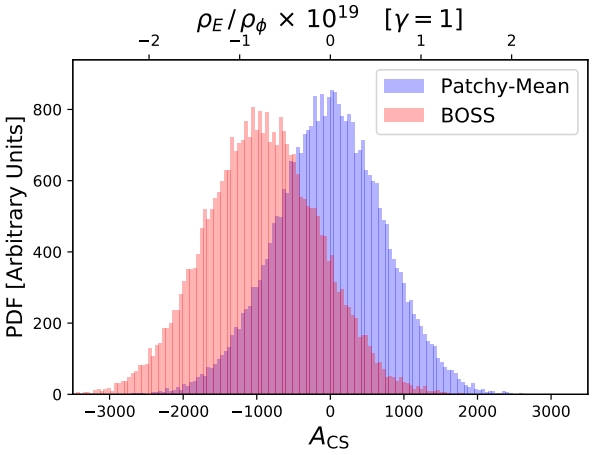

FIG. 6. Constraints on the amplitude of a physical model for parity-violation, derived from the Chern-Simons Lagrangian of (24) and its corresponding parity-odd 4PCF prediction (30). To obtain these distributions, we fit the measured 4PCF multiplets shown in Fig. 2 to a template derived in Appendix A, following compression of both observations and model into a 100-dimensional subspace. Results are given for both the trispectrum amplitude $A_{\rm CS}$ and the corresponding ratio of parity-breaking gauge field and inflaton energy densities, ρ_E/ρ_ϕ, using relation (27) with $|\gamma| = 1$. The 1σ constraints are $A_{\rm CS} = 10 \pm 720$ for the mean of 1000 Patchy mocks (blue) and $A_{\rm CS} = -930 \pm 770$ for the BOSS data (red), both of which are consistent with zero.

(cf. A9). Here, I, J and K are Bessel-weighted integrals over the transfer function and/or primordial power spectrum (A10), $\mathcal{C}_{\ell_1\cdots\ell_N} \equiv \sqrt{(2\ell_1+1)\cdots(2\ell_N+1)}$, and $\mathcal{M}$ is a coupling matrix given in (A11). The 4PCF may thus be computed as a two-dimensional integral, following evaluation of the (radially-binned) I, J and K functions for a range of values of L, ℓ, x and x'. In practice, the 4PCF model is computed in PYTHON, with the various Wigner 3-j and 9-j symbols evaluated using SYMPY.[14]

B. Amplitude Constraints

The importance of the Chern-Simons term in the inflationary Lagrangian of (24) may be quantified by the gauge field energy density, ρ_E/ρ_ϕ, or, equivalently, the parity-odd 4PCF amplitude, $A_{\rm CS}$ (27). To constrain these, we perform parameter inference using the measured 4PCF multiplets of §V and the Chern-Simons model given in (30). For simplicity, we will assume the data to be Gaussian distributed, and work in a compressed subspace containing $N_{\rm eig} = 100$ basis vectors for each of the NGC and SGC regions. In §IV B, a minimum-variance criterion was used to select the basis vectors; here, we instead pick those with maximal signal-to-noise for the Chern-Simons model. The reduced dimensionality facilitates direct use of the Patchy simulations to form the sample covariance (20); to account for the finite number of mocks, we perform inference using the following log-likelihood:

$$-\log L(A_{\rm CS}) = \frac{N_{\rm mocks}}{2} \log\left[1 + \frac{T^2(A_{\rm CS})}{N_{\rm mocks}-1}\right] + \text{const.} \tag{31}$$

This uses the T^2 statistic, defined analogously to (21):

$$T^2(A_{\rm CS}) \equiv (\hat{v}_{\rm data} - A_{\rm CS} v_{\rm CS})^T \, \hat{C}_v^{-1} \, (\hat{v}_{\rm data} - A_{\rm CS} v_{\rm CS}) \,, \tag{32}$$

where $\hat{v}_{\rm data}$ represents the compressed 4PCF data-vector, $\hat{C}_v$ is a sample covariance, and $v_{\rm CS}$ is the compressed 4PCF model of (30), excluding the $A_{\rm CS}$ prefactor. Likelihoods for the NGC and SGC region are constructed separately and multiplied, assuming independence. Here, we perform two analyses; one using the BOSS data, and the second using the mean of $N_{\rm mocks} = 1000$ Patchy mocks. In the latter case, no Chern-Simons contribution should be present.

Fig. 6 shows the resulting constraints on the trispectrum amplitude, whose sign has not been restricted. For the Patchy mean, the 1σ constraint is $A_{\rm CS} = 10 \pm 720$ (centered close to zero, as expected), with $A_{\rm CS} = -930 \pm 770$

[14] Code implementing this calculation is available at github.com/oliverphilcox/Parity-Odd-4PCF, upon paper acceptance.

observed for BOSS. In both cases, we do not detect a parity-violating 4PCF signature, matching the conclusions of §V. If we additionally restrict to $A_{\rm CS} \geq 0$ (as expected from theory), we find the 95% confidence intervals, $A_{\rm CS} < 1000$ and $A_{\rm CS} < 1500$ for the mean-of-Patchy and BOSS datasets respectively. Additionally including tetrahedra with small separations between secondary galaxies (as in §V) does not appreciably improve the constraints, which we justify by noting that the bulk of the signal-to-noise occurs on large scales.

Of greater physical interest are the constraints on the energy densities ρ_E/ρ_ϕ. These may be obtained from the $A_{\rm CS}$ bounds using (27), assuming fiducial values for the inflationary parameters and fixing the coupling strength to $|\gamma| = 1$, giving an equal contribution from the parity-even and parity-odd terms in (24). Using the BOSS CMASS data, we find $\rho_E/\rho_\phi < 8.2 \times 10^{-20}$ at 95% confidence. If $|\gamma|$ is increased to 2, the gauge field production is strongly amplified, and the constraint tightens to $\rho_E/\rho_\phi < 1.8 \times 10^{-33}$. Our results may be compared to those of [31], who considered the possible constraints on the Chern-Simons model from the parity-odd CMB trispectrum. The former work forecasted a 1σ bound on ρ_E/ρ_ϕ of $\sim 10^{-20}$ for a cosmic-variance dominated measurement using $\ell_{\rm max} = 2000$ and $|\gamma| = 1$. Notably, signatures of the gauge field coupling in (24) can be found in other observables, including the parity-even trispectrum, the bispectrum and the direction-dependent power spectrum. However, as noted in [31, Fig. 4], the CMB trispectrum yields *much* stronger bounds on ρ_E/ρ_ϕ than the other observables. For LSS, the parity-odd 4PCF is an optimal place in which to search for such signatures, since the statistic is free from gravitational effects. As the volume of spectroscopic data increases, we expect the constraints on ρ_E/ρ_ϕ to significantly strengthen, especially considering that the signal-to-noise of the Chern-Simons 4PCF (30) scales as $\sqrt{V_{\rm survey}}$, independently of redshift.[15] A survey such as DESI will probe $\sim 100\times$ the BOSS volume [32], and should thus be expected to tighten the constraints on ρ_E/ρ_ϕ (and any other parity-breaking model amplitudes) by roughly an order of magnitude.

VII. SUMMARY AND CONCLUSIONS

Searching for parity-violation provides a unique way to probe new physics occurring in the early Universe, including that of non-standard inflation, baryogenesis, and primordial magnetic field generation. Whilst there is a long history of constraining various parity-breaking phenomena using the CMB [5, 7, 8, 12, 15, 24, 31, 68, 69], few analyses have made use of LSS data. In this work, we have placed the first constraints on scalar-type parity-violation from LSS, using the BOSS CMASS galaxy sample. The isotropic NPCFs are only parity-sensitive if $N > 3$; recent developments in NPCF computation [35] have enabled efficient computation of the galaxy 4PCF, enabling such analyses. To provide a model-agnostic test, we have performed a blind search for parity-violation using the full parity-odd 4PCF (whose expectation value is zero in ΛCDM). Our primary tool has been a non-parametric rank test, comparing the BOSS 4PCF (on scales between $20h^{-1}$Mpc and $160h^{-1}$Mpc) to that of a suite of realistic mock catalogs. This avoids assuming that the 4PCF likelihood is Gaussian, and provides a robust (albeit conservative) test for parity-violation. We found no evidence for parity-violation in BOSS, with a detection probability of 7.8%.

As an additional test, we have performed a classical χ^2-based analysis of the BOSS data, making use of a data compression scheme and a covariance matrix computed from mock catalogs. Furthermore, we use a theoretical Gaussian covariance [40] to facilitate high-fidelity compression; importantly, the results are *not* biased this choice, avoiding a potential systematic error. Post-compression, the empirical χ^2 distribution closely matches that of the theory model, indicating that the assumption of Gaussianity is valid on these scales. For this test, we find a detection probability of 14.7% from BOSS, again showing no evidence for scalar parity-violation. Additionally, this functions as a null test for systematics, since imperfections in the modelling of the survey mask could generate an parity-odd 4PCF; the non-detection found herein (for both simulations and data) suggests that these effects are small.

Finally, we may use the measured 4PCF to bound the amplitudes of physical models of parity-violation. Here, we have considered only a single scenario; a Chern-Simons term in the inflationary Lagrangian, which couples the inflaton to a $U(1)$ gauge field. This leads to a definite prediction for the primordial polyspectra [31, 68], which, with some effort, can be translated into a model for the galaxy 4PCF. Performing a Gaussian likelihood analysis using this template gives a comparable constraint on the ratio of gauge field and inflaton energy densities to that expected from the CMB [31]; $\rho_E/\rho_\phi < 8.2 \times 10^{-20}$ (at 95% confidence), assuming standard inflationary parameters. Similar constraints may be obtained for any other physical model giving a definite prediction for the galaxy 4PCF.

The coming years will lead to an explosion in the volume of LSS data available, and thus a significant tightening of the constraints on physical models that generate parity-violation. Unlike for the gravitational contribution [38], the signal-to-noise of the inflationary 4PCF is not a strong function of redshift, with the constraints being primarily sensitive to the survey volume. To further increase the constraining power, we may fold in additional information,

[15] Note that this differs from the signal-to-noise of the *gravitational* 4PCF, which scales as $[b(z)D(z)]^2\sqrt{V_{\rm survey}}$ [38].

for example using the 5PCF and anisotropic NPCFs (which source additional information regarding vector parity-breaking [28]). Going beyond spectroscopic surveys, it is likely that high-volume observables such as intensity mapping and the Lyman-α forest will tighten these bounds further, surpassing the CMB cosmic variance limit and pinning down a variety of new physics models.

ACKNOWLEDGMENTS

We thank Jiamin Hou for providing us with analytic covariance matrices. We are additionally indebted to Stephon Alexander, Giovanni Cabass, David Spergel and Morgane König for insightful discussions regarding parity-violation, Robert Cahn, Daniel Eisenstein, Jiamin Hou and Zachary Slepian for conversations relating to NPCFs, William Underwood for suggesting the non-parametric statistics of §IV A, and Mikhail Ivanov, Marko Simonović, and Matias Zaldarriaga for general feedback. OHEP acknowledges funding from the WFIRST program through NNG26PJ30C and NNN12AA01C, and thanks the Simons Foundation for additional support.

The authors are pleased to acknowledge that the work reported in this paper was substantially performed using the Princeton Research Computing resources at Princeton University, which is a consortium of groups led by the Princeton Institute for Computational Science and Engineering (PICSciE) and the Office of Information Technology's Research Computing Division.

Appendix A: Derivation of the Chern-Simons 4PCF Model

Below, we sketch the derivation of the parity-odd 4PCF induced by the Chern-Simons coupling of §VI. Our starting point is the general expression given in (29), which is a product of four pieces. By expanding the angular dependence of each term using the isotropic basis functions (§II A), we may compute the full 4PCF efficiently.

To begin, we consider the primordial Chern-Simons trispectrum defined in (26). The angular pieces may be written in terms of isotropic basis functions of three coordinates using [36, Appendix A.2]:

$$(\hat{\boldsymbol{k}}_1\times\hat{\boldsymbol{k}}_3)\cdot\hat{\boldsymbol{s}} = i\frac{\sqrt{2}}{3}(4\pi)^{3/2}\mathcal{P}_{111}(\hat{\boldsymbol{k}}_1,\hat{\boldsymbol{k}}_3,\hat{\boldsymbol{s}}), \qquad \hat{\boldsymbol{k}}_1\cdot\hat{\boldsymbol{k}}_3 = -\frac{1}{\sqrt{3}}(4\pi)^{3/2}\mathcal{P}_{110}(\hat{\boldsymbol{k}}_1,\hat{\boldsymbol{k}}_3,\hat{\boldsymbol{s}}), \tag{A1}$$
$$\hat{\boldsymbol{k}}_1\cdot\hat{\boldsymbol{s}} = -\frac{1}{\sqrt{3}}(4\pi)^{3/2}\mathcal{P}_{101}(\hat{\boldsymbol{k}}_1,\hat{\boldsymbol{k}}_3,\hat{\boldsymbol{s}}), \qquad \hat{\boldsymbol{k}}_1\cdot\hat{\boldsymbol{k}}_3 = -\frac{1}{\sqrt{3}}(4\pi)^{3/2}\mathcal{P}_{011}(\hat{\boldsymbol{k}}_1,\hat{\boldsymbol{k}}_3,\hat{\boldsymbol{s}}).$$

The resulting products of two basis functions can be simplified using [36, §6.3], yielding

$$t(\boldsymbol{k}_1,\boldsymbol{k}_3,\boldsymbol{s}) = -\sqrt{2}A_{\rm CS}(4\pi)^{3/2}P_\zeta(k_1)P_\zeta(k_3)P_\zeta(s) \tag{A2}$$
$$\times\left[\mathcal{P}_{111}(\hat{\boldsymbol{k}}_1,\hat{\boldsymbol{k}}_3,\hat{\boldsymbol{s}}) + \frac{1}{\sqrt{5}}\mathcal{P}_{221}(\hat{\boldsymbol{k}}_1,\hat{\boldsymbol{k}}_3,\hat{\boldsymbol{s}}) + \frac{1}{\sqrt{5}}\mathcal{P}_{212}(\hat{\boldsymbol{k}}_1,\hat{\boldsymbol{k}}_3,\hat{\boldsymbol{s}}) - \frac{1}{\sqrt{5}}\mathcal{P}_{122}(\hat{\boldsymbol{k}}_1,\hat{\boldsymbol{k}}_3,\hat{\boldsymbol{s}})\right],$$

whose radial part is separable in k_1, k_3 and s.

Next, we consider the Dirac delta functions. By rewriting $(2\pi)^3\delta_{\rm D}\left(\boldsymbol{k}_1+\boldsymbol{k}_2-\boldsymbol{s}\right)$ as a complex exponential, inserting plane-wave expansions [70, Eq. 16.63], then performing the angular integral, the function can be expressed as a sum over one-dimensional integrals and isotropic basis functions of three coordinates:

$$(2\pi)^3\delta_{\rm D}\left(\boldsymbol{k}_1+\boldsymbol{k}_2-\boldsymbol{s}\right) = (4\pi)^{5/2}\sum_{L_1L_2L_5} i^{L_1+L_2+L_5}(-1)^{L_5}\mathcal{C}_{L_1L_2L_5}\begin{pmatrix}L_1 & L_2 & L_5\\ 0 & 0 & 0\end{pmatrix}\mathcal{P}_{L_1L_2L_5}(\hat{\boldsymbol{k}}_1,\hat{\boldsymbol{k}}_2,\hat{\boldsymbol{s}}) \tag{A3}$$
$$\times\int_0^\infty x^2dx\, j_{L_1}(k_1x)j_{L_2}(k_2x)j_{L_5}(sx),$$

where $\mathcal{C}_{L_1\ldots L_N}\equiv\sqrt{(2L_1+1)\ldots(2L_N+1)}$, 2×3 matrices are Wigner 3-j symbols and we have used properties of the Gaunt integral [71, Eq. 34.3.22]. Similarly,

$$(2\pi)^3\delta_{\rm D}\left(\boldsymbol{k}_3+\boldsymbol{k}_4+\boldsymbol{s}\right) = (4\pi)^{5/2}\sum_{L_3L_4L_5'} i^{L_3+L_4+L_5'}\mathcal{C}_{L_3L_4L_5'}\begin{pmatrix}L_3 & L_4 & L_5'\\ 0 & 0 & 0\end{pmatrix}\mathcal{P}_{L_3L_4L_5'}(\hat{\boldsymbol{k}}_3,\hat{\boldsymbol{k}}_4,\hat{\boldsymbol{s}}) \tag{A4}$$
$$\times\int_0^\infty x'^2dx'\, j_{L_3}(k_3x')j_{L_4}(k_4x')j_{L_5'}(sx').$$

Note that the integrands are again separable in $\{k_i\}$ and s. Using the approach of [72], they may equivalently be rewritten as infinite sums.

For the transfer functions $M(k,z)Z_1(\boldsymbol{k},z)$, we first expand the redshift-space kernel $Z_1(\boldsymbol{k})$ in spherical harmonics (dropping the redshift dependence for clarity):

$$Z_1(\hat{\boldsymbol{k}};\hat{\boldsymbol{n}}) \equiv b + f(\hat{\boldsymbol{k}}\cdot\hat{\boldsymbol{n}})^2 = 4\pi\sum_{\ell m}\left[\left(b+\frac{f}{3}\right)\delta^{\rm K}_{\ell 0} + \frac{2f}{15}\delta^{\rm K}_{\ell 2}\right]Y^*_{\ell m}(\hat{\boldsymbol{n}})Y_{\ell m}(\hat{\boldsymbol{k}}) \equiv 4\pi\sum_{\ell m} Z_\ell\, Y^*_{\ell m}(\hat{\boldsymbol{n}})Y_{\ell m}(\hat{\boldsymbol{k}}), \tag{A5}$$

for linear bias $b(z)$, growth rate $f(z)$ and line-of-sight $\hat{\boldsymbol{n}}$. Since we consider only isotropic 4PCFs in this work, we can integrate over the LoS orientation (which is equivalent to performing a joint rotation of all $\{\boldsymbol{r}_i\}$). Following some algebra, this leads to a set of isotropic functions of *four* coordinates (see [36] for details):

$$\begin{aligned}\int\frac{d\hat{\boldsymbol{n}}}{4\pi}Z_1(\hat{\boldsymbol{k}}_1;\hat{\boldsymbol{n}})Z_1(\hat{\boldsymbol{k}}_2;\hat{\boldsymbol{n}})Z_1(\hat{\boldsymbol{k}}_3;\hat{\boldsymbol{n}})Z_1(\hat{\boldsymbol{k}}_4;\hat{\boldsymbol{n}}) &= (4\pi)^2\sum_{j_1j_2j_{12}j_3j_4}\begin{pmatrix}j_1 & j_2 & j_{12}\\ 0&0&0\end{pmatrix}\begin{pmatrix}j_{12} & j_3 & j_4\\ 0&0&0\end{pmatrix}Z_{j_1}Z_{j_2}Z_{j_3}Z_{j_4}\\ &\times\mathcal{C}_{j_1j_2j_{12}j_3j_4}\mathcal{P}_{j_1j_2(j_{12})j_3j_4}(\hat{\boldsymbol{k}}_1,\hat{\boldsymbol{k}}_2,\hat{\boldsymbol{k}}_4,\hat{\boldsymbol{k}}_4),\end{aligned} \tag{A6}$$

where $j_i\in\{0,2\}$ and $j_{12}\in\{0,2,4\}$.

The final contribution is from the Fourier basis functions and their permutations, which can be written

$$e^{i(\boldsymbol{k}_1\cdot\boldsymbol{r}_1+\boldsymbol{k}_2\cdot\boldsymbol{r}_2+\boldsymbol{k}_3\cdot\boldsymbol{r}_3)} + 23\text{ perms.} = \sum_H e^{i(\boldsymbol{k}_1\cdot\boldsymbol{r}_{H1}+\boldsymbol{k}_2\cdot\boldsymbol{r}_{H2}+\boldsymbol{k}_3\cdot\boldsymbol{r}_{H3}+\boldsymbol{k}_4\cdot\boldsymbol{r}_{H4})}, \tag{A7}$$

where $\{H1,H2,H3,H4\}$ is one of the 24 permutations of $\{1,2,3,4\}$, and we have introduced $\boldsymbol{r}_4=0$ for convenience. Projecting onto the 4PCF basis functions $\mathcal{P}_{\ell_1\ell_2\ell_3}(\hat{\boldsymbol{r}}_1,\hat{\boldsymbol{r}}_2,\hat{\boldsymbol{r}}_3)$ gives a sum of isotropic functions of four coordinates:

$$\begin{aligned}&\sum_H(4\pi)^{-1/2}\int d\hat{\boldsymbol{r}}_1d\hat{\boldsymbol{r}}_2d\hat{\boldsymbol{r}}_3d\hat{\boldsymbol{r}}_4\,\mathcal{P}^*_{\ell_1\ell_2\ell_3}(\hat{\boldsymbol{r}}_1,\hat{\boldsymbol{r}}_2,\hat{\boldsymbol{r}}_3)e^{i(\boldsymbol{k}_1\cdot\boldsymbol{r}_{H1}+\boldsymbol{k}_2\cdot\boldsymbol{r}_{H2}+\boldsymbol{k}_3\cdot\boldsymbol{r}_{H3}+\boldsymbol{k}_4\cdot\boldsymbol{r}_{H4})}Y_{\ell_4m_4}(\hat{\boldsymbol{r}}_4)\\ &=\sum_H(4\pi)^{7/2}\Phi_H(-i)^{\ell_1+\ell_2+\ell_3}j_{\ell_{H1}}(k_1r_{H1})j_{\ell_{H2}}(k_2r_{H2})j_{\ell_{H3}}(k_3r_{H3})j_{\ell_{H4}}(k_4r_{H4})\mathcal{P}_{\ell_{H1}\ell_{H2}(\ell^*)\ell_{H3}\ell_{H4}}(\hat{\boldsymbol{k}}_1,\hat{\boldsymbol{k}}_2,\hat{\boldsymbol{k}}_3,\hat{\boldsymbol{k}}_4),\end{aligned} \tag{A8}$$

using the plane wave expansion and inserting $\ell_4=m_4=r_4=0$ in the first line. In the second line we include a permutation factor Φ_H, given by $(-1)^{\ell_1+\ell_2+\ell_3}$ if $\{\ell_{H1},\ell_{H2},\ell_{H3},\ell_{H4}\}$ is an odd permutation of $\{\ell_1,\ell_2,\ell_3\}$ (removing the zero element) and unity else. Furthermore, ℓ^* is set by the position of the zero, e.g., $\ell^*=\ell_{H2}$ if $\ell_{H1}=0$, $\ell^*=\ell_{H4}$ if $\ell_{H3}=0$ *et cetera*.

Combining the above results, we obtain

$$\begin{aligned}\zeta_{\ell_1\ell_2\ell_3}(r_1,r_2,r_3) = (4\pi)^{11}\sqrt{2}A_{\rm CS}\,i^{\ell_1+\ell_2+\ell_3}\sum_H\sum_{L_1L_2L_3L_4L_5L_5'}&i^{L_1+L_2+L_3+L_4-L_5+L_5'}\mathcal{C}_{L_1L_2L_3L_4L_5L_5'}\\ &\times\begin{pmatrix}L_1&L_2&L_5\\0&0&0\end{pmatrix}\begin{pmatrix}L_3&L_4&L_5'\\0&0&0\end{pmatrix}\times\mathcal{M}^{\ell_{H1}\ell_{H2}(\ell^*)\ell_{H3}\ell_{H4}}_{L_1L_2L_3L_4L_5L_5'}\\ &\times\int x^2dx\int x'^2dx'\,K_{L_5L_5'}(x,x')I^{\ell_{H1}}_{L_1}(x;r_{H1})J^{\ell_{H2}}_{L_2}(x;r_{H2})I^{\ell_{H3}}_{L_3}(x';r_{H3})J^{\ell_{H4}}_{L_4}(x';r_{H4}),\end{aligned} \tag{A9}$$

defining the integrals:

$$\begin{aligned}I^\ell_L(x;r)\equiv\int_0^\infty\frac{k^2dk}{2\pi^2}M(k)P_\zeta(k)j_L(kx)j_\ell(kr),\qquad J^\ell_L(x;r)\equiv\int_0^\infty\frac{k^2dk}{2\pi^2}M(k)j_L(kx)j_\ell(kr),\\ K_{LL'}(x,x')\equiv\int_0^\infty\frac{s^2ds}{2\pi^2}P_\zeta(s)j_L(sx)j_{L'}(sx').\end{aligned} \tag{A10}$$

In practice, we must integrate the statistic over radial bins of finite width, which corresponds to replacing e.g., $j_\ell(kr)$ with $\bar{j}^b_\ell(k)$ for bin b. The bin-integrated Bessel functions are analytic and can be found in [73, Appendix A].

The coupling matrix in (A9) is given by an integral over five isotropic basis functions of five coordinates:

$$\begin{aligned}\mathcal{M}^{\ell_{H1}\ell_{H2}(\ell^*)\ell_{H3}\ell_{H4}}_{L_1L_2L_3L_4L_5L_5'}\sum_{j_1j_2j_{12}j_3j_4}&\mathcal{C}_{j_1j_2j_{12}j_3j_4}\begin{pmatrix}j_1&j_2&j_{12}\\0&0&0\end{pmatrix}\begin{pmatrix}j_{12}&j_3&j_4\\0&0&0\end{pmatrix}Z_{j_1}Z_{j_2}Z_{j_3}Z_{j_4}\int d\hat{\boldsymbol{k}}_1d\hat{\boldsymbol{k}}_2d\hat{\boldsymbol{k}}_3d\hat{\boldsymbol{k}}_4d\hat{\boldsymbol{s}}\\ &\times\left[\mathcal{P}_{j_1j_2(j_{12})j_3(j_4)j_40}\mathcal{P}_{L_1L_2(L_5)0(L_5)0L_5}\mathcal{P}_{00(0)L_3(L_3)L_4L_5'}\mathcal{P}_{\ell_{H1}\ell_{H2}(\ell^*)\ell_{H3}(\ell_{H4})\ell_{H4}0}\right](\hat{\boldsymbol{k}}_1,\hat{\boldsymbol{k}}_2,\hat{\boldsymbol{k}}_3,\hat{\boldsymbol{k}}_4,\hat{\boldsymbol{s}})\\ &\times\left[\mathcal{P}_{10(1)1(1)01}+\frac{1}{\sqrt{5}}\mathcal{P}_{20(2)2(2)01}+\frac{1}{\sqrt{5}}\mathcal{P}_{20(2)1(2)02}-\frac{1}{\sqrt{5}}\mathcal{P}_{10(1)2(2)02}\right](\hat{\boldsymbol{k}}_1,\hat{\boldsymbol{k}}_2,\hat{\boldsymbol{k}}_3,\hat{\boldsymbol{k}}_4,\hat{\boldsymbol{s}}),\end{aligned} \tag{A11}$$

where we have noted that that isotropic functions of N coordinates may be rewritten in terms of those with $N+M \geq N$ coordinates by inserting a factor $(4\pi)^{M/2}$. Whilst complex, this can be evaluated analytically, making extensive use of the product relation for isotropic basis functions of five coordinates:

$$\mathcal{P}_\Lambda \mathcal{P}_{\Lambda'} = (4\pi)^{-5/2} \sum_{\Lambda''} (-1)^{\Lambda_1''+\Lambda_2''+\Lambda_3''+\Lambda_4''+\Lambda_5''} \mathcal{C}_\Lambda \mathcal{C}_{\Lambda'} \mathcal{C}_{\Lambda''} \prod_{i=1}^{5} \left[\begin{pmatrix} \Lambda_i & \Lambda_i' & \Lambda_i'' \\ 0 & 0 & 0 \end{pmatrix} \right] \mathcal{P}_{\Lambda''} \tag{A12}$$
$$\times \begin{Bmatrix} \Lambda_1 & \Lambda_2 & \Lambda_{12} \\ \Lambda_1' & \Lambda_2' & \Lambda_{12}' \\ \Lambda_1'' & \Lambda_2'' & \Lambda_{12}'' \end{Bmatrix} \begin{Bmatrix} \Lambda_{12} & \Lambda_3 & \Lambda_{123} \\ \Lambda_{12}' & \Lambda_3' & \Lambda_{123}' \\ \Lambda_{12}'' & \Lambda_3'' & \Lambda_{123}'' \end{Bmatrix} \begin{Bmatrix} \Lambda_{123} & \Lambda_4 & \Lambda_5 \\ \Lambda_{123}' & \Lambda_4' & \Lambda_5' \\ \Lambda_{123}'' & \Lambda_4'' & \Lambda_5'' \end{Bmatrix}$$

[36, §6.5], where $\Lambda \equiv \{\Lambda_1, \Lambda_2, (\Lambda_3), \Lambda_4, (\Lambda_{123}), \Lambda_4, \Lambda_5\}$, the curly braces indicate Wigner 9-j symbols and $\mathcal{C}_\Lambda$ involves all elements of Λ. This simplifies considerably when some elements of Λ or Λ' are zero.

[1] T. D. Lee and C. N. Yang, *Question of parity conservation in weak interactions*, *Phys. Rev.* **104** (1956) 254.
[2] A. D. Sakharov, *Violation of CP Invariance, C Asymmetry, and Baryon Asymmetry of the Universe*, *Soviet Journal of Experimental and Theoretical Physics Letters* **5** (1967) 24.
[3] H. Davoudiasl, R. Kitano, G. D. Kribs, H. Murayama and P. J. Steinhardt, *Gravitational Baryogenesis*, *Phys. Rev. Lett.* **93** (2004) 201301 [hep-ph/0403019].
[4] S. Alexander, *Inflationary birefringence and baryogenesis*, *International Journal of Modern Physics D* **25** (2016) 1640013 [1604.00703].
[5] S. H. S. Alexander, *Is cosmic parity violation responsible for the anomalies in the WMAP data?*, *Physics Letters B* **660** (2008) 444 [hep-th/0601034].
[6] T. Liu, X. Tong, Y. Wang and Z.-Z. Xianyu, *Probing P and CP violations on the cosmological collider*, *Journal of High Energy Physics* **2020** (2020) 189 [1909.01819].
[7] A. Lue, L. Wang and M. Kamionkowski, *Cosmological Signature of New Parity-Violating Interactions*, *Phys. Rev. Lett.* **83** (1999) 1506 [astro-ph/9812088].
[8] N. Bartolo and G. Orlando, *Parity breaking signatures from a Chern-Simons coupling during inflation: the case of non-Gaussian gravitational waves*, JCAP **2017** (2017) 034 [1706.04627].
[9] S. Alexander and N. Yunes, *Chern-Simons modified general relativity*, Phys. Rep. **480** (2009) 1 [0907.2562].
[10] D. Grasso and H. R. Rubinstein, *Magnetic fields in the early Universe*, Phys. Rep. **348** (2001) 163 [astro-ph/0009061].
[11] Planck Collaboration, P. A. R. Ade, N. Aghanim, M. Arnaud, F. Arroja, M. Ashdown et al., *Planck 2015 results. XIX. Constraints on primordial magnetic fields*, A&A **594** (2016) A19 [1502.01594].
[12] M. Shiraishi, *Parity violation of primordial magnetic fields in the CMB bispectrum*, JCAP **2012** (2012) 015 [1202.2847].
[13] L. Pogosian and M. Wyman, *B-modes from cosmic strings*, *Phys. Rev. D* **77** (2008) 083509 [0711.0747].
[14] D. Regan and M. Hindmarsh, *The bispectrum of matter perturbations from cosmic strings*, JCAP **2015** (2015) 008 [1411.2641].
[15] I. Y. Rybak and L. Sousa, *CMB anisotropies generated by cosmic string loops*, *Phys. Rev. D* **104** (2021) 023507 [2104.08375].
[16] J. L. Cook and L. Sorbo, *Particle production during inflation and gravitational waves detectable by ground-based interferometers*, *Phys. Rev. D* **85** (2012) 023534 [1109.0022].
[17] P. Adshead, J. Giblin, John T., T. R. Scully and E. I. Sfakianakis, *Gauge-preheating and the end of axion inflation*, JCAP **2015** (2015) 034 [1502.06506].
[18] Y. Minami and E. Komatsu, *New Extraction of the Cosmic Birefringence from the Planck 2018 Polarization Data*, *Phys. Rev. Lett.* **125** (2020) 221301 [2011.11254].
[19] S. E. Clark, C.-G. Kim, J. C. Hill and B. S. Hensley, *The Origin of Parity Violation in Polarized Dust Emission and Implications for Cosmic Birefringence*, *arXiv e-prints* (2021) arXiv:2105.00120 [2105.00120].
[20] U. Seljak and M. Zaldarriaga, *Signature of Gravity Waves in the Polarization of the Microwave Background*, *Phys. Rev. Lett.* **78** (1997) 2054 [astro-ph/9609169].
[21] R. G. Crittenden, P. Natarajan, U.-L. Pen and T. Theuns, *Discriminating Weak Lensing from Intrinsic Spin Correlations Using the Curl-Gradient Decomposition*, ApJ **568** (2002) 20 [astro-ph/0012336].
[22] S. M. Carroll, G. B. Field and R. Jackiw, *Limits on a Lorentz- and parity-violating modification of electrodynamics*, *Phys. Rev. D* **41** (1990) 1231.
[23] F. Schmidt, N. E. Chisari and C. Dvorkin, *Imprint of inflation on galaxy shape correlations*, JCAP **2015** (2015) 032 [1506.02671].
[24] M. Kamionkowski and T. Souradeep, *Odd-parity cosmic microwave background bispectrum*, *Phys. Rev. D* **83** (2011) 027301 [1010.4304].
[25] N. Kaiser, *Clustering in real space and in redshift space*, MNRAS **227** (1987) 1.
[26] A. J. S. Hamilton, *Linear Redshift Distortions: a Review*, vol. 231, p. 185. 1998. 10.1007/978-94-011-4960-0_17.

[27] C. Bonvin, R. Durrer, N. Khosravi, M. Kunz and I. Sawicki, *Redshift-space distortions from vector perturbations*, JCAP **2018** (2018) 028 [1712.00052].

[28] D. Jeong and F. Schmidt, *The Odd-Parity Galaxy Bispectrum*, *arXiv e-prints* (2019) arXiv:1906.05198 [1906.05198].

[29] D. Munshi, A. Heavens, A. Cooray, J. Smidt, P. Coles and P. Serra, *New optimized estimators for the primordial trispectrum*, MNRAS **412** (2011) 1993 [0910.3693].

[30] K. M. Smith, L. Senatore and M. Zaldarriaga, *Optimal analysis of the CMB trispectrum*, *arXiv e-prints* (2015) arXiv:1502.00635 [1502.00635].

[31] M. Shiraishi, *Parity violation in the CMB trispectrum from the scalar sector*, *Phys. Rev. D* **94** (2016) 083503 [1608.00368].

[32] DESI Collaboration, A. Aghamousa, J. Aguilar, S. Ahlen, S. Alam, L. E. Allen et al., *The DESI Experiment Part I: Science,Targeting, and Survey Design*, *arXiv e-prints* (2016) arXiv:1611.00036 [1611.00036].

[33] LSST Science Collaboration, P. A. Abell, J. Allison, S. F. Anderson, J. R. Andrew, J. R. P. Angel et al., *Lsst science book, version 2.0*, 2009.

[34] C. G. Sabiu, B. Hoyle, J. Kim and X.-D. Li, *Graph Database Solution for Higher-order Spatial Statistics in the Era of Big Data*, ApJS **242** (2019) 29 [1901.00296].

[35] O. H. E. Philcox, Z. Slepian, J. Hou, C. Warner, R. N. Cahn and D. J. Eisenstein, *ENCORE: Estimating Galaxy N-point Correlation Functions in $\mathcal{O}(N_{\rm g}^2)$ Time*, *arXiv e-prints* (2021) arXiv:2105.08722 [2105.08722].

[36] R. N. Cahn and Z. Slepian, *Isotropic N-Point Basis Functions and Their Properties*, *arXiv e-prints* (2020) arXiv:2010.14418 [2010.14418].

[37] O. H. E. Philcox and Z. Slepian, *Efficient Computation of N-point Correlation Functions in D Dimensions*, *arXiv e-prints* (2021) arXiv:2106.10278 [2106.10278].

[38] O. H. E. Philcox, J. Hou and Z. Slepian, "A First Detection of the Connected 4-Point Correlation Function of Galaxies using the BOSS CMASS Sample." in prep.

[39] M. Liguori, E. Sefusatti, J. R. Fergusson and E. P. S. Shellard, *Primordial Non-Gaussianity and Bispectrum Measurements in the Cosmic Microwave Background and Large-Scale Structure*, *Advances in Astronomy* **2010** (2010) 980523 [1001.4707].

[40] J. Hou, R. Cahn, O. Philcox and Z. Slepian, "Analytic Gaussian Covariance Matrices for Galaxy N-Point Correlation Functions." in prep.

[41] T. L. Smith and M. Kamionkowski, *Probability distribution for non-Gaussianity estimators constructed from the CMB trispectrum*, *Phys. Rev. D* **86** (2012) 063009 [1203.6654].

[42] C. Hahn, F. Beutler, M. Sinha, A. Berlind, S. Ho and D. W. Hogg, *Likelihood non-Gaussianity in large-scale structure analyses*, MNRAS **485** (2019) 2956 [1803.06348].

[43] S. D. Landy and A. S. Szalay, *Bias and Variance of Angular Correlation Functions*, ApJ **412** (1993) 64.

[44] I. Szapudi and A. S. Szalay, *A New Class of Estimators for the N-Point Correlations*, ApJ **494** (1998) L41.

[45] Z. Slepian, D. J. Eisenstein, J. R. Brownstein, C.-H. Chuang, H. Gil-Marín, S. Ho et al., *Detection of baryon acoustic oscillation features in the large-scale three-point correlation function of SDSS BOSS DR12 CMASS galaxies*, MNRAS **469** (2017) 1738 [1607.06097].

[46] S. Alam, F. D. Albareti, C. Allende Prieto, F. Anders, S. F. Anderson, T. Anderton et al., *The Eleventh and Twelfth Data Releases of the Sloan Digital Sky Survey: Final Data from SDSS-III*, ApJS **219** (2015) 12 [1501.00963].

[47] D. J. Eisenstein, D. H. Weinberg, E. Agol, H. Aihara, C. Allende Prieto, S. F. Anderson et al., *SDSS-III: Massive Spectroscopic Surveys of the Distant Universe, the Milky Way, and Extra-Solar Planetary Systems*, AJ **142** (2011) 72 [1101.1529].

[48] K. S. Dawson, D. J. Schlegel, C. P. Ahn, S. F. Anderson, É. Aubourg, S. Bailey et al., *The Baryon Oscillation Spectroscopic Survey of SDSS-III*, AJ **145** (2013) 10 [1208.0022].

[49] F. Beutler, H.-J. Seo, S. Saito, C.-H. Chuang, A. J. Cuesta, D. J. Eisenstein et al., *The clustering of galaxies in the completed SDSS-III Baryon Oscillation Spectroscopic Survey: anisotropic galaxy clustering in Fourier space*, MNRAS **466** (2017) 2242 [1607.03150].

[50] H. A. Feldman, N. Kaiser and J. A. Peacock, *Power-Spectrum Analysis of Three-dimensional Redshift Surveys*, ApJ **426** (1994) 23 [astro-ph/9304022].

[51] F.-S. Kitaura, S. Rodríguez-Torres, C.-H. Chuang, C. Zhao, F. Prada, H. Gil-Marín et al., *The clustering of galaxies in the SDSS-III Baryon Oscillation Spectroscopic Survey: mock galaxy catalogues for the BOSS Final Data Release*, MNRAS **456** (2016) 4156 [1509.06400].

[52] S. A. Rodríguez-Torres, C.-H. Chuang, F. Prada, H. Guo, A. Klypin, P. Behroozi et al., *The clustering of galaxies in the SDSS-III Baryon Oscillation Spectroscopic Survey: modelling the clustering and halo occupation distribution of BOSS CMASS galaxies in the Final Data Release*, MNRAS **460** (2016) 1173 [1509.06404].

[53] Z. Slepian and D. J. Eisenstein, *Computing the three-point correlation function of galaxies in O(N2̂) time*, MNRAS **454** (2015) 4142 [1506.02040].

[54] F. Sosa Nuñez and G. Niz, *On the fast random sampling and other properties of the three point correlation function in galaxy surveys*, JCAP **2020** (2020) 021 [2006.05434].

[55] M. Vargas-Magaña, S. Ho, A. J. Cuesta, R. O'Connell, A. J. Ross, D. J. Eisenstein et al., *The clustering of galaxies in the completed SDSS-III Baryon Oscillation Spectroscopic Survey: theoretical systematics and Baryon Acoustic Oscillations in the galaxy correlation function*, MNRAS **477** (2018) 1153 [1610.03506].

[56] D. Wadekar and R. Scoccimarro, *Galaxy power spectrum multipoles covariance in perturbation theory*, *Phys. Rev. D* **102**

(2020) 123517 [1910.02914].
[57] O. H. E. Philcox and D. J. Eisenstein, *Estimating covariance matrices for two- and three-point correlation function moments in Arbitrary Survey Geometries*, MNRAS **490** (2019) 5931 [1910.04764].
[58] M. M. Ivanov, M. Simonović and M. Zaldarriaga, *Cosmological parameters from the BOSS galaxy power spectrum*, JCAP **2020** (2020) 042 [1909.05277].
[59] A. Chudaykin, M. M. Ivanov, O. H. E. Philcox and M. Simonović, *Nonlinear perturbation theory extension of the Boltzmann code CLASS*, *Phys. Rev. D* **102** (2020) 063533 [2004.10607].
[60] A. F. Heavens, R. Jimenez and O. Lahav, *Massive lossless data compression and multiple parameter estimation from galaxy spectra*, MNRAS **317** (2000) 965 [astro-ph/9911102].
[61] R. Scoccimarro, *The Bispectrum: From Theory to Observations*, ApJ **544** (2000) 597 [astro-ph/0004086].
[62] J. Alsing and B. Wandelt, *Generalized massive optimal data compression*, MNRAS **476** (2018) L60 [1712.00012].
[63] O. H. E. Philcox, M. M. Ivanov, M. Zaldarriaga, M. Simonović and M. Schmittfull, *Fewer mocks and less noise: Reducing the dimensionality of cosmological observables with subspace projections*, *Phys. Rev. D* **103** (2021) 043508 [2009.03311].
[64] J. Wishart and M. S. Bartlett, *The generalised product moment distribution in a normal system*, *Proceedings of the Cambridge Philosophical Society* **29** (1933) 260.
[65] J. Hartlap, P. Simon and P. Schneider, *Why your model parameter confidences might be too optimistic. Unbiased estimation of the inverse covariance matrix*, A&A **464** (2007) 399 [astro-ph/0608064].
[66] E. Sellentin and A. F. Heavens, *Parameter inference with estimated covariance matrices*, MNRAS **456** (2016) L132 [1511.05969].
[67] C. Eckart and G. Young, *The approximation of one matrix by another of lower rank*, *Psychometrika* **1** (1936) 211.
[68] N. Bartolo, S. Matarrese, M. Peloso and M. Shiraishi, *Parity-violating CMB correlators with non-decaying statistical anisotropy*, JCAP **2015** (2015) 039 [1505.02193].
[69] L. Sorbo, *Parity violation in the Cosmic Microwave Background from a pseudoscalar inflaton*, JCAP **2011** (2011) 003 [1101.1525].
[70] G. Arfken, H. Weber and F. Harris, *Mathematical Methods for Physicists: A Comprehensive Guide*. Elsevier Science, 2013.
[71] NIST, *NIST Digital Library of Mathematical Functions*. DLMF.
[72] O. H. E. Philcox and Z. Slepian, *An Exact Integral-to-Sum Relation for Products of Bessel Functions*, *arXiv e-prints* (2021) arXiv:2104.10169 [2104.10169].
[73] O. H. E. Philcox and D. J. Eisenstein, *Computing the small-scale galaxy power spectrum and bispectrum in configuration space*, MNRAS **492** (2020) 1214 [1912.01010].